JAERI-M
84-002

ELECTRON PROBE MICRO-ANALYSIS OF IRRADIATED TRISO-COATED UO_2 PARTICLES (II)

February 1984

Kazuo MINATO, Toru OGAWA, Kousaku FUKUDA
Katsuichi IKAWA and Kazumi IWAMOTO

日本原子力研究所
Japan Atomic Energy Research Institute

JAERI-Mレポートは，日本原子力研究所が不定期に公刊している研究報告書です。
入手の問合わせは，日本原子力研究所技術情報部情報資料課（〒319-11茨城県那珂郡東海村）あて，お申しこしください。なお，このほかに財団法人原子力弘済会資料センター（〒319-11 茨城県那珂郡東海村日本原子力研究所内）で複写による実費頒布をおこなっております。

JAERI-M reports are issued irregularly.
Inquiries about availability of the reports should be addressed to Information Section, Division of Technical Information, Japan Atomic Energy Research Institute, Tokai-mura, Naka-gun, Ibaraki-ken 319-11, Japan.

編集兼発行　日本原子力研究所
印　　刷　いばらき印刷㈱

JAERI-M 84-002

Electron Probe Micro-Analysis of Irradiated Triso-coated UO_2 particles (II)

Kazuo MINATO, Toru OGAWA, Kousaku FUKUDA,
Katsuichi IKAWA and Kazumi IWAMOTO

Department of Fuels and Materials Research,
Tokai Research Establishment, JAERI

(Received January 6, 1984)

Irradiated Triso coated UO_2 particles were observed by means of electron probe microanalyzer. Although the present experiment was preliminary, palladium accumulation at inner surface of the SiC layers and palladium penetration into the SiC layers were observed. Palladium was detected at all levels of palladium amount in a particle from 1.1×10^{15} to 3.6×10^{15} atoms/particle. Although palladium was detected on both hot and cold sides of the particle, the amount of paladium and the number of accumulation positions on the cold side were greater than those on the hot side of the particle. Cerium, tellurium, and barium were also detected at inner surface of the SiC layers as well as in the buffer-PyC layers. Detection of chlorine was tried in the coating layers but was prevented by the epoxy resin, since it contained chlorine.

Keywords:
HTGR Fuel, Coated Fuel Particles, EPMA, Fission Products, Post-Irradiation Examination, Silicon Carbide, Palladium, Cerium

JAERI－M 84－002

照射済Triso被覆UO_2粒子のEPMA（Ⅱ）

日本原子力研究所東海研究所燃料工学部
湊　和生・小川　徹・福田幸朔
井川勝市・岩本多實

（1984年1月6日受理）

照射済Triso被覆UO_2粒子をEPMAを用いて観察した。この実験は初歩的なものであったが，パラジウムのSiC層内面における蓄積，およびSiC層中への侵入が見られた。パラジウム量が1粒子あたり1.1×10^{15}～3.6×10^{15} atom／particleの粒子において，パラジウムのSiC層内面における蓄積が見られた。パラジウムの蓄積は，粒子の高温側でも低温側でも見られたが，蓄積量および蓄積個所は，低温側の方が多かった。セリウム，テルル，およびバリウムは，バッファーPyC層中ばかりでなく，SiC層内面でも検出された。被覆層中の塩素の検出を試みたが，使用した樹脂に塩素が含まれていたため，妨害された。

Contents

目　　次

1. INTRODUCTION

Triso coated fuel particles for High Temperature Gas-cooled Reactors (HTGR) consist of microspherical fuel (kernel) which is surrounded by four layers of pyrolytic carbon (PyC) and silicon carbide (SiC). These coating layers have functions of retaining gaseous and solid fission products within the particles, and thus are regarded as the miniature pressure vessel and the diffusion barrier for the fission products.

Interactions between fission products and SiC coating layer have been observed in irradiated coated fuel particles[1-6] and studied by out-of-reactor experiments[6-12] in past few years. Study on fission products-SiC interactions is of great importance because these interactions lead to the loss of ability to retain fission products within the particles. By the works on the behavior of fission products in the particles, it was found that the main fission products which interact with the SiC layer were the rare earths and palladium (Pd). The rare earths-SiC interaction was observed in both carbide and carbide-oxide fuels. This interaction, however, is not considered to occur in the fuel with O/U>1.1, since sufficient oxygen stabilizes the rare earths as oxides in the kernel[2]. On the other hand, palladium-SiC interaction was observed in both carbide and oxide fuels. Fission yields for palladium from ^{235}U and ^{239}Pu are 1.578% and 15.893%, respectively[13]. The latter is about ten times as large as the former. Consequently, low-enriched uranium (LEU) yields larger amount of palladium than high-enriched uranium (HEU), even

when their burnups are the same.

For development of VHTR, JAERI has carried out the irradiation examination of the Triso coated low-enriched uranium (E.U.<20%) dioxide (UO_2) particles. Therefore, in the JAERI coated particles occurrence of the Pd-SiC interaction is more probable than that of the rare earths-SiC interaction for the reason mentioned above.

In the present experiment, irradiated coated fuel particles were observed by means of Electron Probe Micro-Analyzer (EPMA) for the first time in JAERI. As the present experiment was preliminary, the experimental data were described in detail in the present report for the future experiments. The present report is the second one on the EPMA experiments and deals with fission product behavior in the coating layers. The fission product behavior in the kernel has been described in the first report[14].

2. EXPERIMENTAL

Samples used in the present experiment were Triso coated UO_2 particles. These particles were taken from five production batches and irradiated in five capsules in the Japan Materials Testing Reactor (JMTR). Some particles were irradiated as loose particles and the others as fuel compacts. Description of the kernel and coating characteristics of the particles is given in Table 2.1. Irradiation data of the samples are summarized in Table 2.2, where the samples are designated by both names of capsule and particle. Irradiation temperatures of each sample are shown in Figs. 2.1 through 2.5. Irradiation temperature at inner surfaces was higher than that at outer surfaces of the compacts, as shown in Figs. 2.4 and 2.5. For this reason, temperature gradient in the particles irradiated as fuel compacts could be estimated roughly. On the other hand, direction of temperature gradient in the particles irradiated as loose particles could not be known, except for the particles where the kernel exhibited migration.

Samples were transported from Hot Laboratory of Tokai Research Establishment to Hot Laboratory of Oarai Research Establishment and then prepared for the electron probe X-ray microanalysis. Several particles or small pieces of compacts were mounted in epoxy resin and polished to the midplane of the particles by standard ceramographic technique. In the case of 75FP2A-1 compact, the particles were removed from the compact, which had been disintegrated electrolytically, prior to the polishing. All polished

particles were observed by optical microscope. Through the optical observation, particles were selected for electron probe X-ray microanalysis. Numbers of the particles observed by optical microscope and by EPMA are summarized in Table 2.3. Gold (Au) was then deposited on the polished surfaces in order to avoid the charging during observation by EPMA.

Shield type EPMA(*) was used, which was installed at Oarai Hot Laboratory. The details of the analyzer have been described in the first report(14).

(*) JEOL-JRXA501

3. RESULTS

3.1 73F-13A.3A(74FC1)

Three particles of 3A were observed by EPMA. Although the polished surface condition of the particles was not suitable for detailed observation of Pd-SiC interaction because the IPyC/SiC interfaces could not be seen clearly, palladium was detected at inner surface of the SiC layers of these particles.

Secondary electron image (SEI) of 3A-1 particle is shown in Fig. 3.1. The kernel did not exhibit migration in this particle. Secondary electron image and backscattered electron image (BEI,COMPO) plus Pd-L_α X-ray image are shown in Fig. 3.2 (a) and (b), respectively. Palladium accumulated circumferentially at inner surface of the SiC layer.

Calsium (Ca) was detected in the IPyC layer of 3A-1 particle. It was considered that calsium had beed included in the kernel as impurity and migrated toward the layers. Secondary electron image of the part where calsium was detected is shown in Fig. 3.3. Energy dispersive X-ray analysis identified calsium, silicon (Si), and cesium (Cs) on the point marked in Fig. 3.3. Result of the analysis is shown in Fig. 3.4. Line scans for Ca-K_α and Si-K_α X-rays indicated that calsium and silicon distributed together, which is seen in Fig. 3.5.

The kernel exhibited migration in 3A-2 particle. Palladium accumulated locally at inner surface of the SiC layer on the cold side of the particle.

Secondary electron image and Pd-$L\alpha$ X-ray image of the part are shown in Fig. 3.6 (a) and (b), respectively. Wavelength dispersive X-ray analysis was conducted on the palladium accumulation point and the result is shown in Fig. 3.7. The analysis identified ruthenium (Ru) and rhodium (Rh) as well as palladium. Chlorine (Cl) was considered to be impurity in the resin contained in the gaps between the layers. Result of energy dispersive X-ray analysis on the same point is shown in Fig. 3.8, which indicates that calsium is also contained in it.

The kernel exhibited migration in 3A-3 particle. Palladium accumulated at inner surface of the SiC layer on the cold side of the particle. Secondary electron image, Si-$K\alpha$, and Pd-$L\alpha$ X-ray images of the cold side of the particle are shown in Fig. 3.9 (a) through (c), respectively. Backscattered electron image of the layer is shown in Fig. 3.10, where analyzed points are marked. Results of energy dispersive X-ray analysis are shown in Fig. 3.11 (a) through (c). White precipitates near the inner surface of the SiC layer contained palladium, cesium, and tellurium (Te). On the other hand, white precipitates near the inner surface of the IPyC layer contained silicon and calsium, but not palladium.

It was examined whether palladium accumulated on the hot side of the particle or not. Secondary electron images and Pd-$L\alpha$ X-ray images of both hot and cold sides of the particle are shown in Fig. 3.12 (a) through (d), respectively. Results of energy dispersive analysis on the marked points in Fig. 3.12 (a) are shown in Fig. 3.13 (a) and (b). From these figures, palladium accumulation on the hot side of the particle was not distinguished. White precipitates at inner surface of the IPyC layer on the

hot side of the particle was identified as uranium (U).

3.2 73F-13A.5A(74FC1)

Two particles of 5A were observed by EPMA. No palladium was detected in the coating layers of both particles.

Secondary electron image of 5A-1 particle is shown in Fig. 3.14. The kernel did not exhibit migration and all coating layers were intact. Energy dispersive X-ray analysis was carried out on each coating layer and the results are shown in Fig. 3.15 (a) through (f). Characteristic distribution of fission products in the coating layers can be seen in Fig. 3.15. Xenon (Xe), cesium, tellurium, and ruthenium were found in the buffer-PyC layer. Small amount of silicon and uranium were also detected in the buffer-PyC layer. In the IPyC layer, small amount of cesium and uranium as well as silicon were detected. Xenon and tellurium were found to be retained within the buffer-PyC layer. At inner surface of the SiC layer and in the SiC layer fission product was hardly detected, which indicated that most of fission products were retained within the particle. Silicon was found in the OPyC layer.

Line scans across the coating layers of intact coated particles were conducted and the result is shown in Fig. 3.16. Xenon distributed in the buffer-PyC layer and was retained within it. Cesium was detected in the SiC layer as well as in the buffer-PyC and IPyC layers. Barium (Ba), neodymium (Nd), and ruthenium were distributed in both buffer-PyC and IPyC layers. Detection of strontium (Sr) was difficult since wavelengths for Sr-Lα and

Si-K_α X-rays are 6.86280 Å and 7.12542 Å, respectively, and the intensity of Si-K_α X-ray is very strong at the SiC layers. For this reason, apparent intensity of Sr-L_α X-ray became strong at the SiC layer.

3.3 73F-13A.5B(74FC1H)

Two particles of 5B were observed by EPMA. No palladium was detected in the coating layers of both particles.

Aluminium (Al) and calsium were detected in the coating layers of 5B-1 particle. Both elements were considered to be impurities in the kernel. Backscattered electron image, Si-K_α, Al-K_α, and Ca-K_α X-ray images are shown in Fig. 3.17 (a) through (d), respectively. Aluminium and calsium distributed mainly in the buffer-PyC and IPyC layers. Energy dispersive X-ray analysis was conducted on the points marked in Fig. 3.17 (a) and the results are shown in Fig. 3.18 (a) through (c). This analysis showd that aluminium, calsium, and uranium distributed to the cracks in the SiC layer, though it could not be clarified whether these elements had interacted with the SiC layer or not.

3.4 75F-5A.75FP2A-1

Two particles from 75FP2A-1 compact were observed by EPMA. These particles were irradiated as fuel compact and removed from it before polishing. Palladium was detected at inner surface of the SiC layers of both particles.

Optical ceramograph of 75FP2A-1-1 particle is shown in Fig. 3.19, where palladium accumulation positions are marked. The kernel did not exhibit migration and the buffer-PyC layer cracked radially in this particle. Palladium accumulated locally at inner surface of the SiC layer. As shown in Fig. 3.19, palladium distributed on half side of the particle.

Optical ceramograph of 75FP2A-1-2 particle is shown in Fig. 3.20. The kernel did not exhibit migration in this particle. Optical ceramograph, secondary electron image, Si-Kα, Pd-Lα, and Ba-Lα X-ray images of the part where palladium accumulated are shown in Fig. 3.21 (a) through(e), respectively. Palladium accumulated circumferentially at inner surface of the SiC layer. Palladium could be seen as white spots in the secondary electron image though white spots were not always palladium. White spots at halfway depth of the IPyC layer were not identified as palladium but as barium and silicon, which is shown in Fig. 3.22. White spots seen in the secondary electron image could not be seen in the optical ceramograph. Result of line scan for Pd-Lα across the coating layers is shown in Fig. 3.23. It was observed from the figure that palladium not only accumulated at inner surface of the SiC layer but also penetrated into the SiC layer by about 1 μm. The relation between palladium and voids seen in the SiC layer could not be clarified.

3.5 75F-4A.760PC3

Two particles of 760PC3 were observed by EPMA. Palladium was detected in the coating layers of both particles. The kernels exhibited migration in

both particles, which had been irradiated as loose particles.

Optical ceramograph of 760PC3-1 particle is shown in Fig. 3.24, where palladium accumulation positions are marked. Although palladium accumulated on both cold and hot sides of the particle, the amount of palladium and the number of accumulation positions on the cold side were greater than those on the hot side of the particle. White precipitates were seen on the cold side of the particle. Optical ceramograph, Si-Kα, Pd-Lα, Te-Lα, and Ce-Lα X-ray images are shown in Fig. 3.25 (a) through (e), respectively. Results of energy dispersive X-ray analysis on the marked points in Fig. 3.25 (a) are shown in Fig. 3.26 (a) and (b). White precipitates at inner surface of the SiC layer and in it seen in Fig. 3.25 (a) were identified as palladium and silicon. On the other hand, white precipitates in the buffer-PyC layer were identified as tellurium and cerium. By optical micrography the depth of palladium penetration into the SiC layer was observed to be about 9 μm. Secondary electron images of Pd-SiC interaction area are shown in Fig. 3.27 (a) and (b). Palladium penetrated into the SiC layer and inner surface of the SiC layer was corroded.

Secondary electron image of 760PC3-2 particle is shown in Fig. 3.28. Palladium was detected on the cold side of the particle. Backscattered electron image and Pd-Lα X-ray image of the cold side of the particle are shown in Fig. 3.29 (a) and (b), respectively. Palladium accumulation in this particle was not distinguished compared with that in 760PC3-1 particle. Many white precipitates containing no palladium were distributed near the SiC layer. Backscattered electron image of the part is shown in Fig. 3.30. Results of energy dispersive X-ray analysis on the points marked

in Fig. 3.30 are shown in Fig. 3.31 (a) and (b). These precipitates were found to contain cerium, barium, silicon, and aluminium. Chlorine in Fig. 3.31 (b) was considered to be impurity in the epoxy resin.

3.6 77F-4A.76FP1A-9

Three particles in 76FP1A-9 compact were observed by EPMA. Palladium accumulated at inner surface of the SiC layers, but its penetration into the SiC layers was not detected in these particles. Optical ceramograph of the piece of the compact is shown in Fig. 3.32 (a). Particles with black kernels seen in the compact are not fuel particles but particles with SiC kernel, which were blended in order to adjust the heat rate of the compact.

Optical ceramographs of 76FP1A-9-1 and 76FP1A-9-2 particles are shown in Fig. 3.32 (b) and (c), respectively, where palladium accumulation positions are marked. Both the amount of palladium and the number of accumulation positions were small. Palladium accumulated only on the cold side of the particle.

3.7 79LF-19A.B-10(790PC)

Five particles in B-10 compact were observed by EPMA. Palladium accumulated at inner surface of the SiC layers of these particles. Optical ceramograph of the piece of the compact is shown in Fig. 3.33 (a). This compact also contained the particles with SiC kernel for the same reason as in the case of 76FP1A-9 compact.

Optical ceramograph of B-10-1 particle is shown in Fig. 3.33 (b), where palladium accumulation positions are marked. Palladium accumulated on half side of the particle. Not only accumulation but also penetration into the SiC layer was detected in this particle. Secondary electron and Pd-$L\alpha$ X-ray images of the part where the penetration was detected are shown in Fig. 3.34 (a) and (b), respectively. Palladium could be seen as white spots in the optical ceramograph. Typical result of line scan for Pd-$L\alpha$ X-ray across the coating layers is shown in Fig. 3.35. The deepest palladium penetration into the SiC layer was observed to be about 2 μm by the line scan. Although a small white spot could be seen about 6 μm into the SiC layer in the optical ceramograph, this spot could not be identified since the spot was too small.

Palladium accumulated at inner surface of the SiC layers, but its penetration into the SiC layer was not detected in other four particles.

4. DISCUSSION

4.1 Palladium

Palladium was detected in the coating layers of all observed Triso coated UO_2 particles except for 73F-13A.5A and 5B particles whose polished surfaces were not in good condition. Observations of palladium in the coating layers are summarized as follows: (1) palladium accumulated locally or circumferentially at inner surface of the SiC layers, (2) palladium penetrated locally into the SiC layer, (3) although palladium accumulated on both hot and cold sides of the particle, the amount of palladium and the number of accumulation positions on the cold side were greater than those on the hot side of the particle, and (4) palladium was detected at all levels of palladium amount in a particle from 1.1×10^{15} to 3.6×10^{15} atoms/particle.

Behavior of palladium in the coating layers observed in the present experiment was similar to that observed by several workers[3-6,10-12] though the relation between palladium accumulation positions and temperature gradient was not consistent. Lauf[11] conducted out-of-reactor temperature gradient heating test on the Triso coated palladium doped UO_2 particles and observed the SiC corrosion particularly on the cold sides of the particles. Montgomery et al.[6] observed palladium accumulation on both hot and cold sides of the irradiated Triso coated UO_2 particles after out-of-reactor temperature gradient heating test. On the other hand,

Pearson et al.[10] concluded that the palladium penetration rate was faster on the hot side than that on the cold side of the particle.

As for dependence of palladium amount in a particle on Pd-SiC interaction, Tiegs[5] observed Pd-SiC interaction at all levels of palladium amount from 1.9×10^{15} to 2.0×10^{16} atoms/particle. In the present experiment, Pd-SiC interaction was observed in the particle with palladium amount 1.1×10^{15} atoms/particle. From these observations, no threshold amount seemed to be necessary for occurrence of palladium penetration into the SiC layer.

Although palladium penetration rate into the SiC layer could not be obtained in the present experiment because of small number of observed particles, palladium penetration depths were estimated by the reported rate equations which are

(1) $X(\mu m/h) = 46.2 \exp(-1.358\times10^5/8.314T)$ [5]

(2) $X(\mu m/h^{0.5}) = 1197 \exp(-1.24\times10^5/8.314T)$, $T(°C)$ [15]

(3) $X(\mu m/h) = 2114 \exp(-1.795\times10^5/8.314T)$ [6]

(4) $X(\mu m^2/h) = 7{,}957\times10^5 \exp(-2.369\times10^5/8.314T)$ [6]

(5) $X(\mu m/h) = 114.84 \exp(-1.28\times10^5/8.314T)$ [12]

(6) $X(\mu m/h) = 4.2\times10^7 \exp(-3.283\times10^5/8.314T)$, $(T>1689K)$

$6.43 \exp(-1.08\times10^5/8.314T)$, $(T<1689K)$ [16].

Irradiation temperatures shown in Fig. 2.1 through 2.5 were used to calculate the penetration depths. The results are given in Table 4.1. Calculated values were found to be greater than observed values except the cases of 75F-4A.760PC3 particles.

These rate equations were based on various experiments. Equation (1)

was based on the accelerated irradiation experiments. Equation (2) was derived without palladium penetration measurement in order to explain irradiation behavior of the particles quantitatively. Equations (3) and (4) were based on accelerated and real time irradiation experiments and out-of-reactor temperature gradient heating experiments on simulated and irradiated particles. Equation (5) was based on out-of-reactor temperature gradient heating experiments on simulated particles. Equation (6) was based on accelerated and real time irradiation experiments and out-of-reactor temperature gradient heating experimens on irradiated particles. As described above, these rate equations were based on various experiments and some of these equations were based on not only Pd-SiC but also rare earths-SiC interaction data (eqs. (3), (4), and (6)).

Comparing these rate equations, the penetration rate based on accelerated irradiation experiment was faster than that based on real time irradiation experiment[16], and that based on out-of-reactor temperature gradient heating experiment was faster than that based on accelerated irradiation experiment. It should be noted that the temperature gradient heating experiment yielded the faster penetration rate.

760PC3-1 particle was irradiated as loose particle and the kernel exhibited migration, which indicated that the temperature gradient in the particle was steep. Deep palladium penetration into the SiC layer observed in 760PC3-1 particle may be attributed to the steep temperature gradient in the particle.

Palladium behavior in the irradiated particles should be studied further by electron probe microanalysis and optical ceramography.

4.2 Other fission products

Cerium, one of the rare earth elements, was detected at inner surface of the SiC layers as well as in the buffer-PyC layers. Other rare earth elements were hardly detected in the coating layers though fission yields for La, Ce, and Nd from ^{235}U are 6.385%, 12.183%, and 20.640%, respectively. The fission yields from ^{239}Pu are almost the same as those from ^{235}U. Förthmann et al.[17] have observed from line scans that cerium and neodymium accumulated at inner surface of the SiC layer of irradiated Triso coated UO_2 particles. It should be noted that the rare earth elements were detected at inner surface of the SiC layer of the UO_2 particles. Although the release rate of the rare earth elements from UO_2 kernels was considered to be very small[18], interaction between the rare earths and the SiC layer may have to be taken into account even in the UO_2 particles.

It was observed that tellurium precipitated in the buffer-PyC layer on the cold side of the particle. This was consistent with the observation by Förthmann et al.[17] that tellurium was found to be preferentially precipitated in the buffer-PyC layer on one side of the particle. Tellurium was detected also at inner surface of the SiC layer in the present experiment. Förthmann et al.[17] and Brown et al.[19] found no tellurium at inner surface of the SiC layers.

Barium was detected at inner surface of the SiC layers as well as in the buffer-PyC layers, which indicated that barium was not retained by the dense PyC layer. At inner surface of the SiC layer barium seemed to form a compound containing silicon. Accumulation of barium at inner surface of the

SiC layer was also observed by Förthmann et al.[17]

4.3 Impurities

Unexpected elements, calsium and aluminium, which could not be introduced during sample preparation, were detected in 74FC1 and 760PC3 particles. As mentioned already, these elements were considered to be impurities in the fuel kernels. Since calsium and aluminium interact with SiC[20,21], it is necessary to avoid these elemens in the fabrication of the fuel particles.

Detection of chlorine was tried in the coating layers, for chlorine might have been introduced during pyrolysis of methyltrichlorosilane (CH_3SiCl_3) in the SiC coating process. The presence of chlorine causes fission product transport due to the formation of fission product chlorides[22]. By this transport process, fission products–SiC interactions must be accelerated. Chlorine was detected in the coating layers of some particles in the present experiment. But it could not be concluded that chlorine had been introduced into the particles during the coating process, since chlorine was also detected in the epoxy resin which had been poured into the gaps between the coating layers during polishing process. It is essential to use the resin with no chlorine in order to study the chlorine behavior.

5. CONCLUSIONS

Irradiated Triso coated UO_2 particles were observed by means of electron probe microanalyzer. The following behaviors of fission products in the coating layers were found though the present experiment was preliminary:

(1) Palladium accumulated locally at inner surface of the SiC layers.

(2) Palladium penetrated locally into the SiC layers.

(3) Although palladium accumulated on both hot and cold sides of the particle, the amount of palladium and the number of accumulation positions on the cold side were greater than those on the hot side of the particle.

(4) Palladium was detected at inner surface of the SiC layer at all levels of palladium amount in a particle from 1.1×10^{15} to 3.6×10^{15} atoms/particle.

(5) Cerium, tellurium, and barium were detected at inner surface of the SiC layers as well as in the buffer–PyC layers.

(6) Detection of chlorine was tried in the coating layers but was prevented by the epoxy resin, which had been poured into the gaps between the coating layers during polishing process, since the epoxy resin contained chlorine.

ACKNOWLEDGEMENTS

The authors wish to express their thanks to Mr. M. Shimizu, Mr. Y. Tayama, Mr. T. Onozaki, Mr. Y. Onuma, and Mr. T. Iwai, engineers of Hot Labolatory of Oarai Research Establishment, for their preparation of the samples and operation of the electron probe microanalyzer. They also wish to express their thanks to Mr. K. Ishimoto, General Manager of Hot Laboratory of Department of Research Reactor Operation, for his management of preparation and transport of the samples.

REFERENCES

(1) C. B. Scott et al., GA-A-13827 (1976).

(2) F. J. Homan et al., Nucl. Technol., 35 ,428 (1977).

(3) T. N. Tiegs et al., ORNL-5510 (1979).

(4) T. N. Tiegs and J. M. Robbins, ORNL-5539 (1979).

(5) T. N. Tiegs, ORNL/TM-7203 (1980).

(6) F. Montgomery et al., DOE/ET/35300-T3 (1981).

(7) C. L. Smith, J. Am. Ceram. Soc., 62, 600 (1979).

(8) R. L. Pearson et al., ORNL/TM-6741 (1979).

(9) R. L. Pearson et al., CONF-770708 (1977).

(10) R. L. Pearson et al., ORNL/TM-6991 (1980).

(11) R. J. Lauf, ORNL/TM-7393 (1980).

(12) R. L. Pearson et al., ORNL/TM-8059 (1982).

(13) B. F. Rider and M. E. Meek, NEDO-12154-2 (1977).

(14) T. Ogawa et al., to be published in JAERI-M (1983).

(15) K. Bongartz and H. Nabielek, C4/2, SMiRT (1981).

(16) HTGR Generic Technology Program, GA-A-15842 (1980).

(17) R. Förthmann et al., in "Thermodynamics of Nuclear Materials 1974" (IAEA,Vienna), P. 147 (1975).

(18) R. Förthmann, Jül-1541 (1978).

(19) P. E. Brown and R. L. Faircloth, J. Nucl. Mater., 59, 29 (1976).

(20) V. A. Pankov, from Chemical Abstracts, 89, 92990m (1978).

(21) A. A. Kortel, from Chemical Abstracts, 76, 144186g (1972).

(22) H. Grübmeier et al., Jül-1382 (1977).

Table 2.1 Characteristics of samples observed by EPMA.

sample	kernel			buffer-PyC		IPyC		SiC		OPyC	
	diameter (μm)	density (%T.D.)	^{235}U enrichment (%)	thickness (μm)	density (Mg/m^3)	thickness (μm)	density (Mg/m^3)	thickness (μm)	density (Mg/m^3)	thickness (μm)	density (Mg/m^3)
74FC1	493	96	8.0	43	1.09	32	1.80	28	3.20	42	1.83
75FP2A	505	97	4.0	44	1.06	27	1.89	27	3.20	45	1.87
76OPC3	599	95	12.0	59	1.19	30	1.86	26	3.21	45	1.86
76FP1A	602	96	4.0	60	1.20	31	1.86	25	3.21	43	1.84
79OPC	606	96	19.9	64	1.11	32	1.82	26	3.20	46	1.82

Table 2.2 Irradiation data of samples observed by EPMA.

sample		irradiation				burnup	Pu fission[2]	Pd amount	
		hole	form[1]	time (day)	temperature (°C)	(%FIMA)	(%)	(atom/particle)	(atom/cm^2-SiC)
73F-13A	3A(74FC1)	K-6	P	111.2	see Fig.2.1	4.4	26	3.6×10^{15}	2.8×10^{17}
73F-13A	5A(74FC1)	K-6	P	111.2	see Fig.2.1	3.93	23	2.9×10^{15}	2.3×10^{17}
73F-13A	5B(74FC1H)[3]	K-6	P	111.2	see Fig.2.1	3.88	22	2.8×10^{15}	2.2×10^{17}
75F-5A	75FP2A-1	F-11	24C	78.0	see Fig.2.2	1.40	23	1.1×10^{15}	8.2×10^{16}
75F-4A	76OPC3	M-6	P	83.1	see Fig.2.3	2.41	4	1.4×10^{15}	7.2×10^{16}
77F-4A	76FP1A-9	I-12	36C	101.0	see Fig.2.4	1.8	30	2.8×10^{15}	1.5×10^{17}
79LF-19A	B-10(79OPC)	OGL-1	24C	142.1	see Fig.2.5	3.07	2	1.5×10^{15}	8.0×10^{16}

1) P:loose particle, 24C:compact(24mm in outer diam. and 8mm in inner diam.), 36C:compact(36mm in outer diam. and 18mm in inner diam.)

2) estimated by the method reported in JAERI-M 83-152 (1983)

3) 74FC1 particles were heated at 1800°C for 1 hour before irradiation.

Table 2.3 Numbers of observed coated fuel particles.

sample		number of particles observed	
		by optical microscope	by EPMA
73F-13A	3A(74FC1)	10	3
73F-13A	5A(74FC1)	5	5
73F-13A	5B(74FC1H)	5	2
75F-5A	75FP2A-1	10	2
75F-4A	76OPC3	10	2
77F-4A	76FP1A-9	5	3
79LF-19A	B-10(79OPC)	20	5

Table 4.1 Observed and estimated Pd penetration into SiC layer.

sample		observed (μm)	estimated[a] (μm)					
			(1)	(2)	(3)	(4)	(5)	(6)
73F-13A	3A(74FC1)	< 1	8.1	7.2	21.7	31.7	33.7	30.7
73F-13A	5A(74FC1)	*[b]	2.9	1.9	5.4	12.7	12.6	3.1
73F-13A	5B(74FC1H)	*	2.9	1.9	5.4	12.7	12.6	3.1
75F-5A	75FP2A-1	~1	5.7	4.9	12.6	27.1	24.3	9.6
75F-4A	76OPC3	~9	3.3	3.0	6.4	20.3	14.7	3.8
77F-4A	76FP1A-9	< 1	1.2-0.5	0.4-0.1	1.5-0.4	5.0-2.1	5.8-2.3	1.7-0.8
79LF-19A	B-10(79OPC)	~2	7.2-4.3	3.9-2.0	13.3-6.8	27.1-17.4	31.5-19.6	7.7-5.1
Reference(1350°Cx440days)		——	20.8	6.5	37.3	46.8	92.1	22.7

a) by reported rate equations;
(1): T.N.Tiegs, ORNL/TM-7203(1980), (2): K.Bongartz et al., SMiRT C4/2(1981),
(3): F.Montgomery, DOE/ET/35300-T3(1981), (4): F.Montgomery, DOE/ET/35300-T3(1981),
(5): R.L.Pearson et al., ORNL/TM-8059(1982), (6): Semiannual report, GA-A-15606(1979)

b) Palladium was not detected.

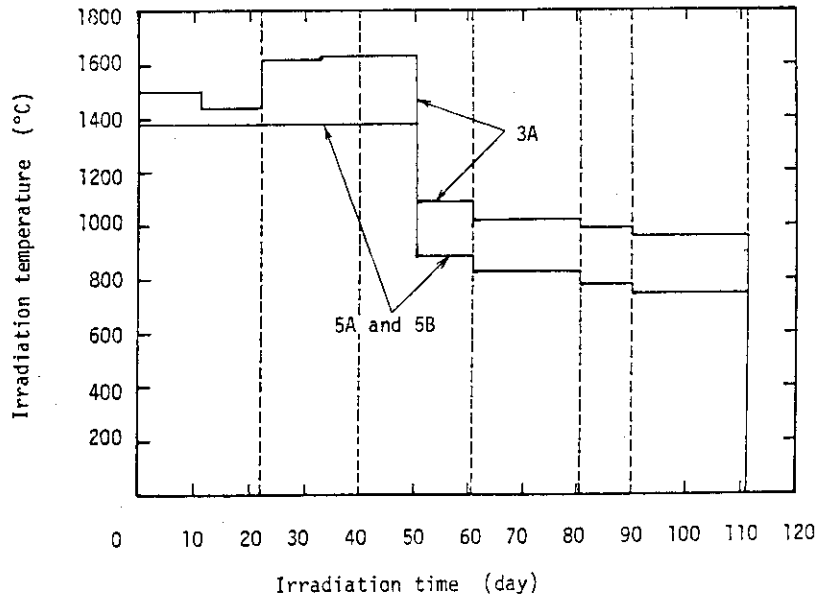

Fig. 2.1 Irradiation temperature of 73F-13A.3A, 5A, and 5B particles.

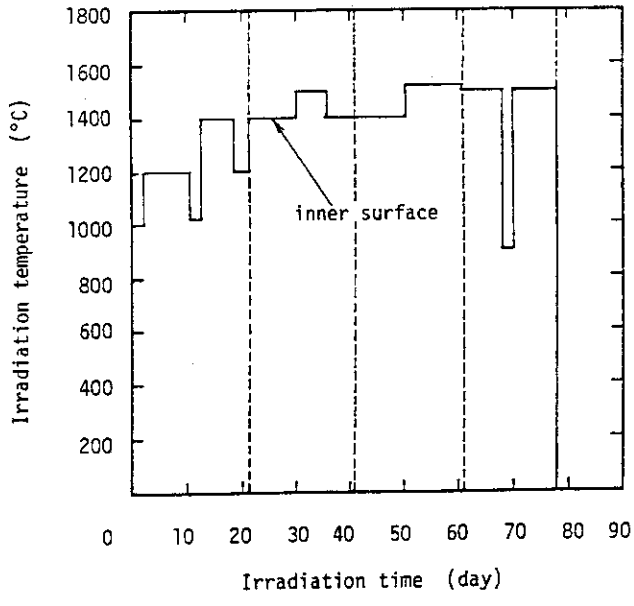

Fig. 2.2
Irradiation temperature of 75F-5A.75FP2A-1 compact.

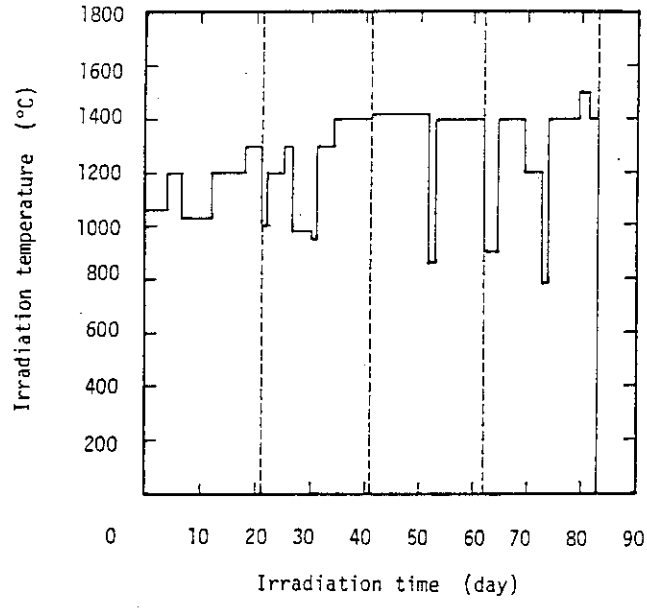

Fig. 2.3
Irradiation temperature of 75F-4A.76OPC3 particles.

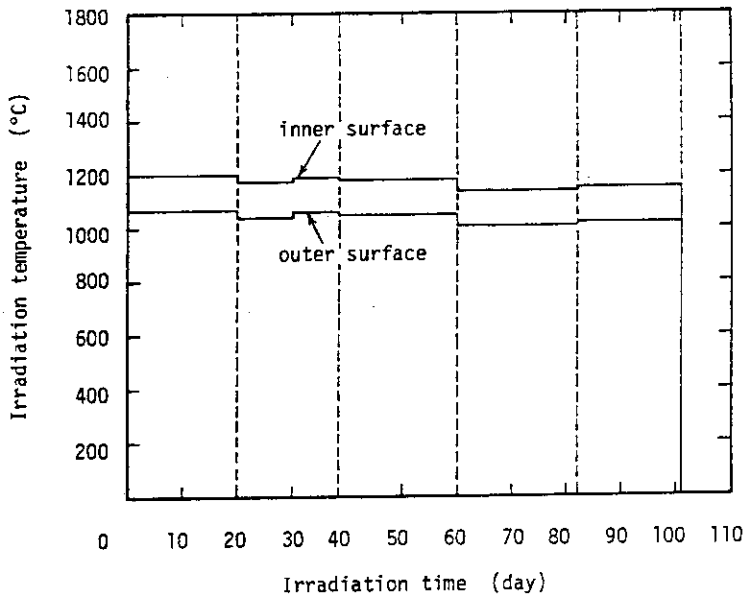

Fig. 2.4 Irradiation temperature of 77F-4A.76FP1A-9 compact.

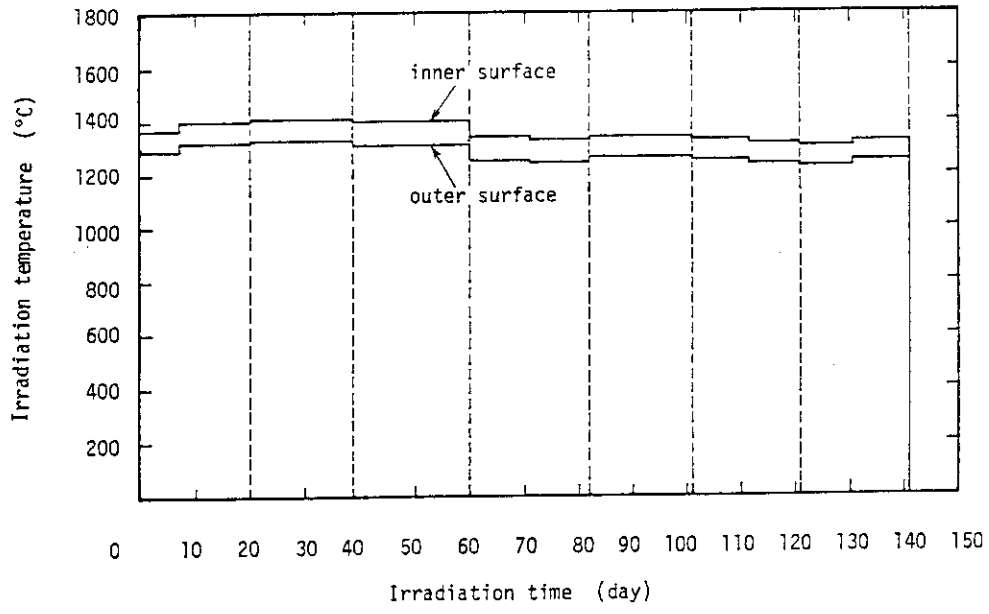

Fig. 2.5 Irradiation temperature of 79LF-19A.B-10(79OPC) compact.

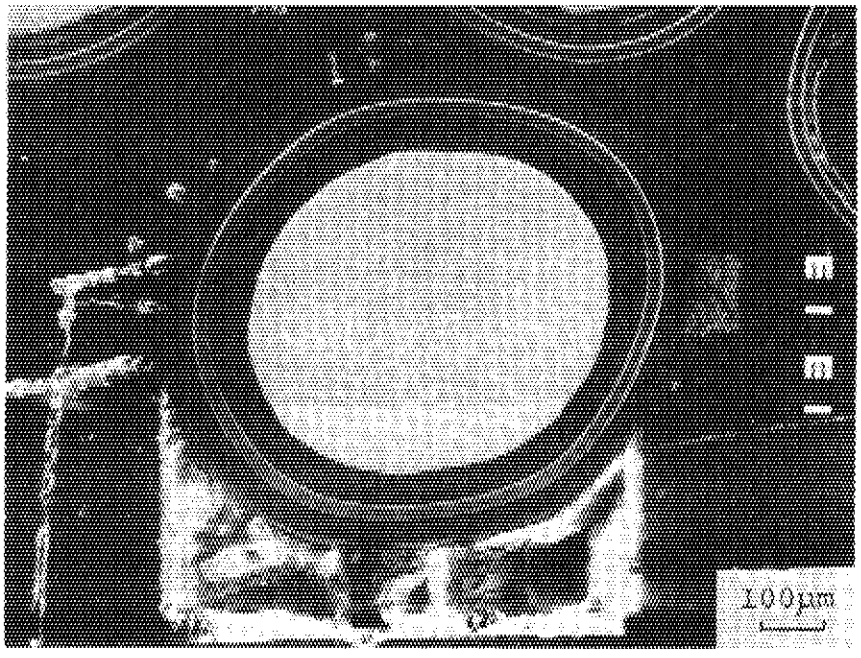

Fig. 3.1 Secondary electron image of 3A-1 particle irradiated in 73F-13A capsule.

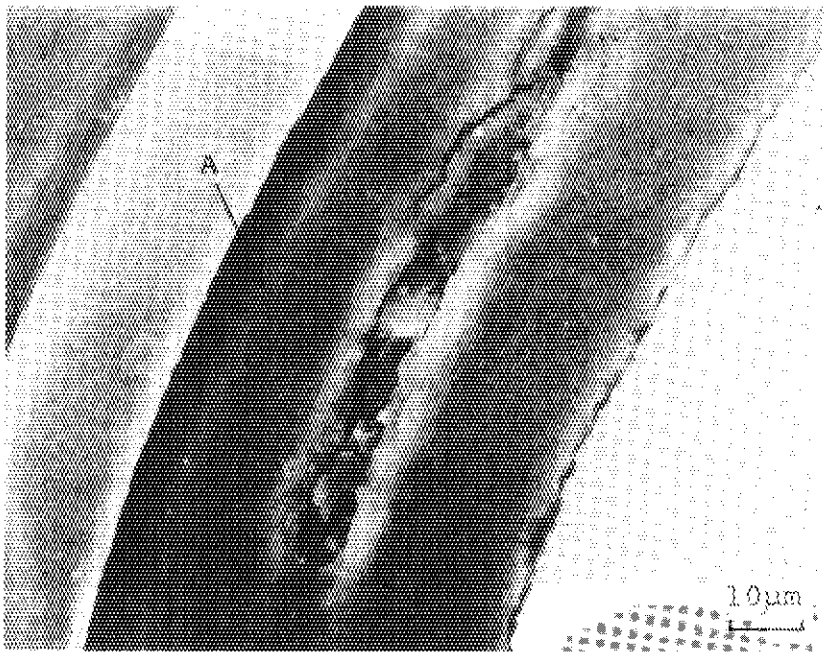

Fig. 3.3 Secondary electron image of the coating layers of 3A-1 particle irradiated in 73F-13A capsule. Letter A indicates X-ray analyzed point.

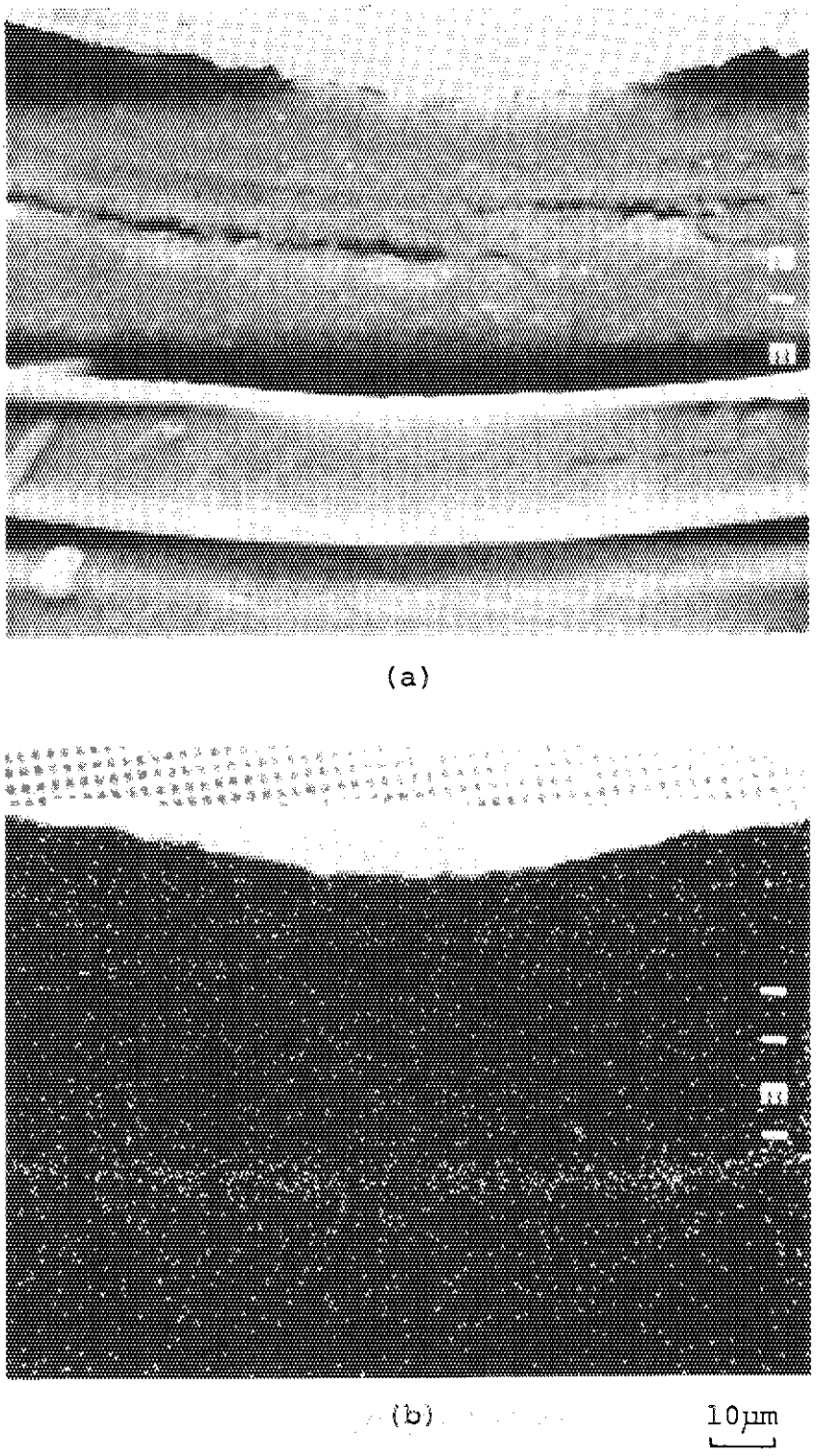

Fig. 3.2 Palladium accumulation at inner surface of the SiC layer of 3A-1 particle irradiated in 73F-13A capsule. (a) Secondary electron image; (b) Backscattered electron plus Pd-Lα image.

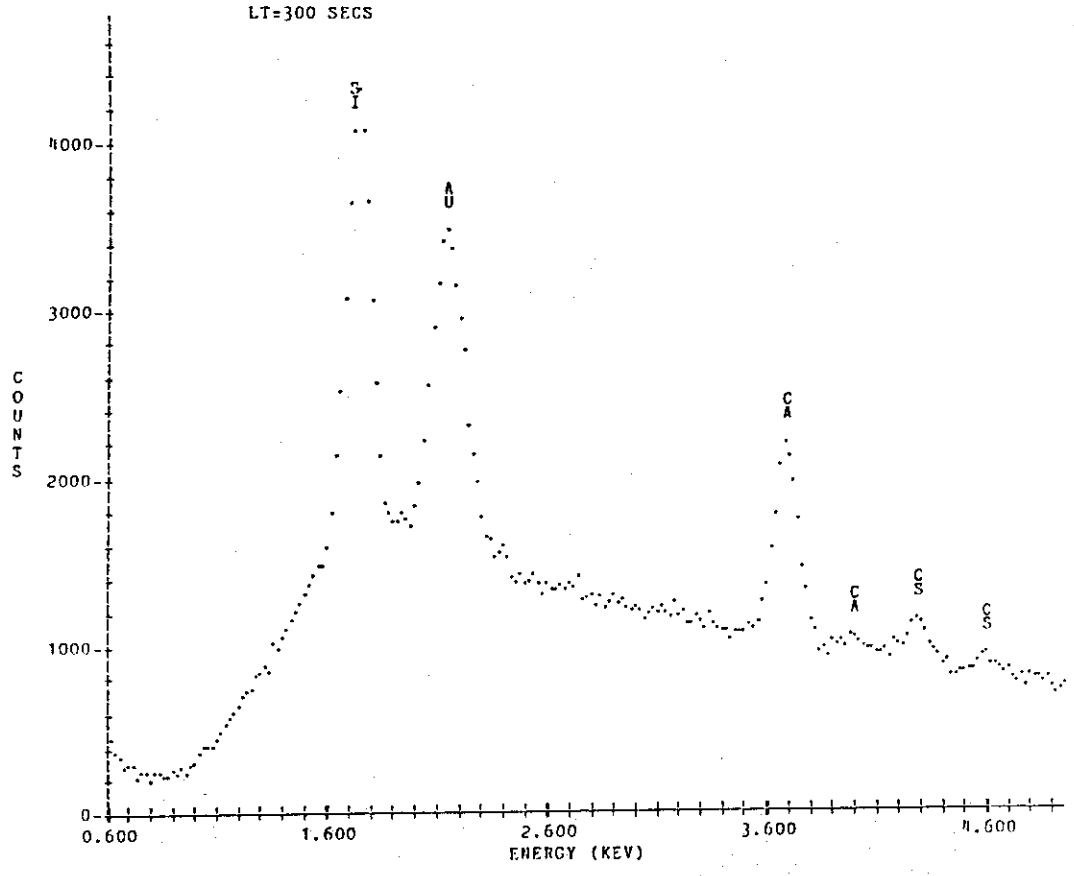

Fig. 3.4 Energy-dispersive X-ray analysis on the point 'A' marked in Fig. 3.3.

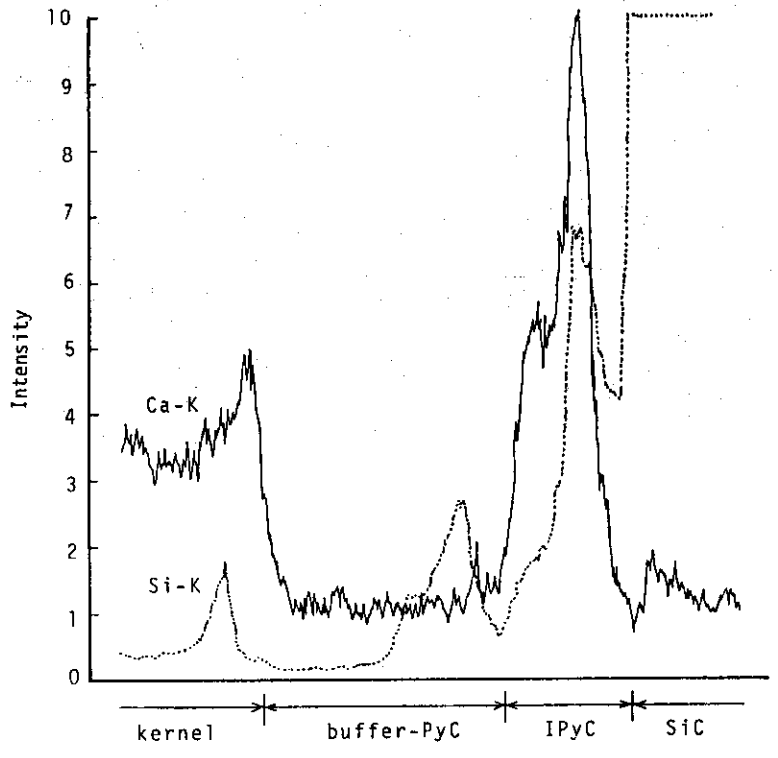

Fig. 3.5 Line scans for calsium and silicon across the coating layers of 73F-13A.3A-1 particle.

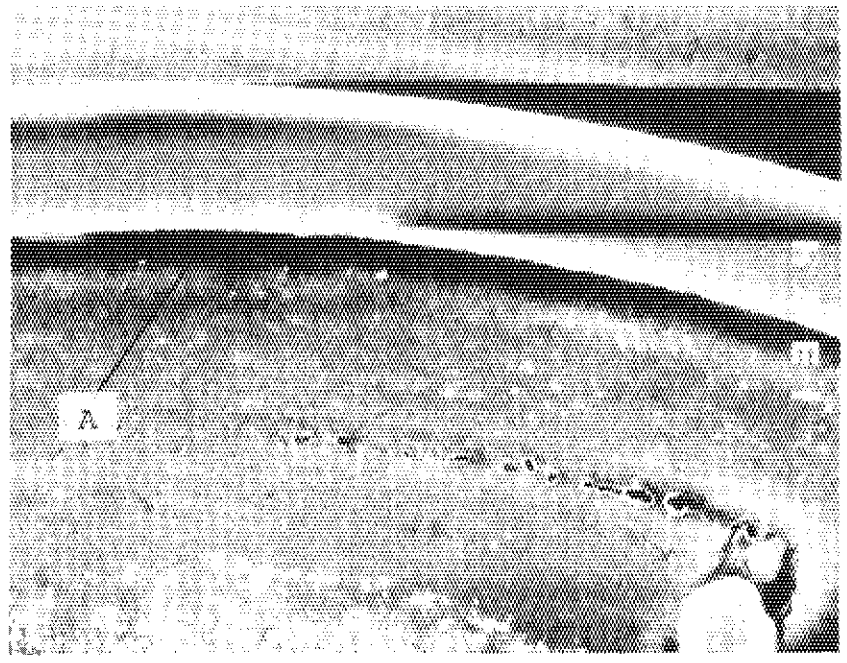

(a)

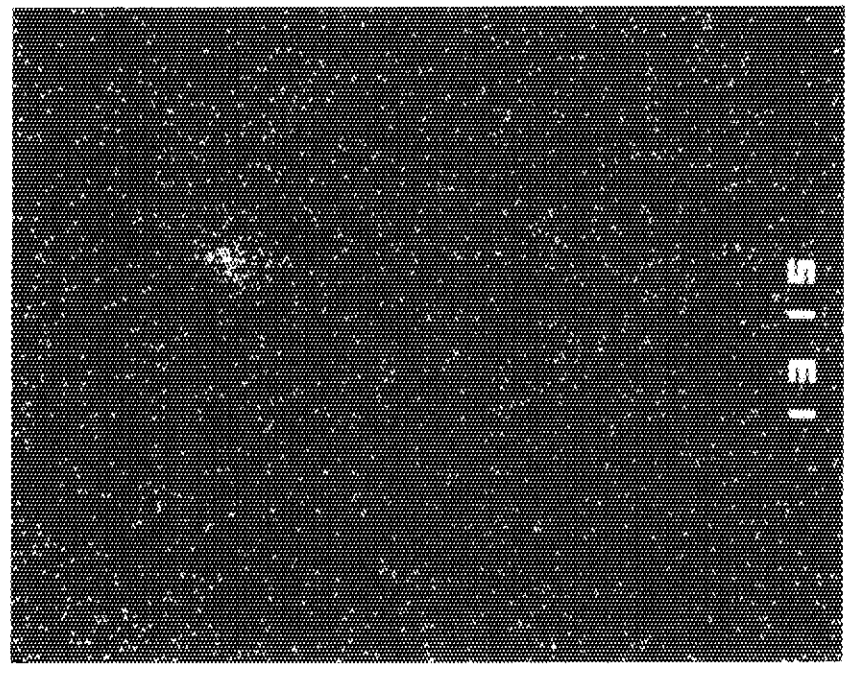

(b)

10μm

Fig. 3.6 Palladium accumulation at inner surface of the SiC layer on the cold side of 3A-2 particle irradiated in 73F-13A capsule. Letter A indicates X-ray analyzed point. (a) Secondary electron image; (b) Pd-Lα image.

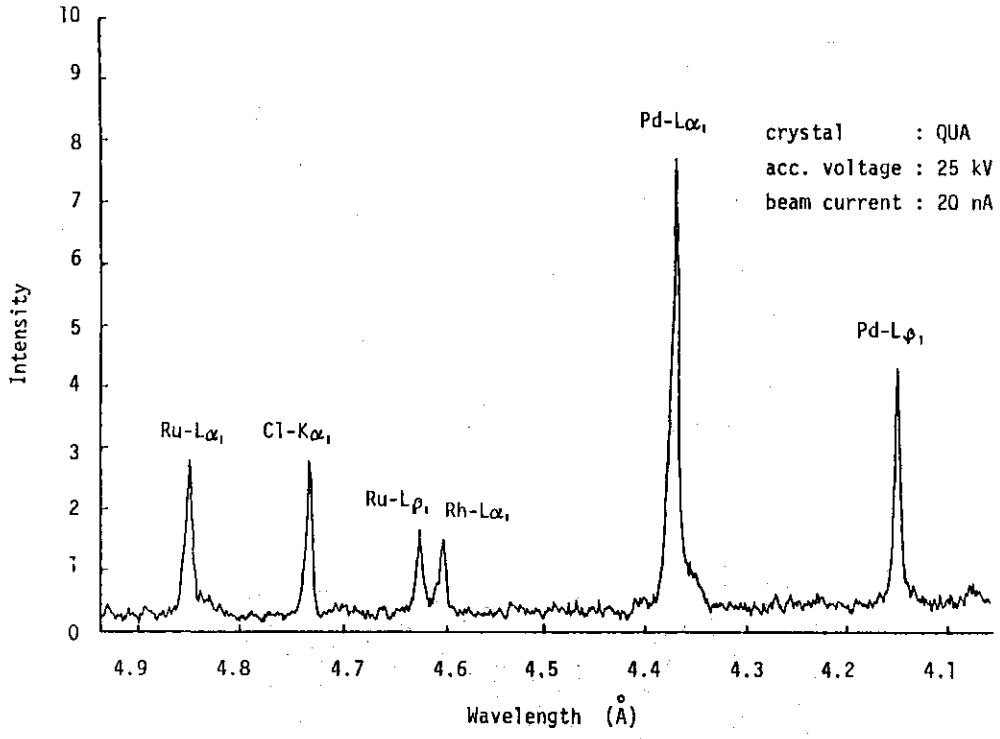

Fig. 3.7 Wavelength-dispersive X-ray analysis on the point 'A' marked in Fig. 3.6 (a).

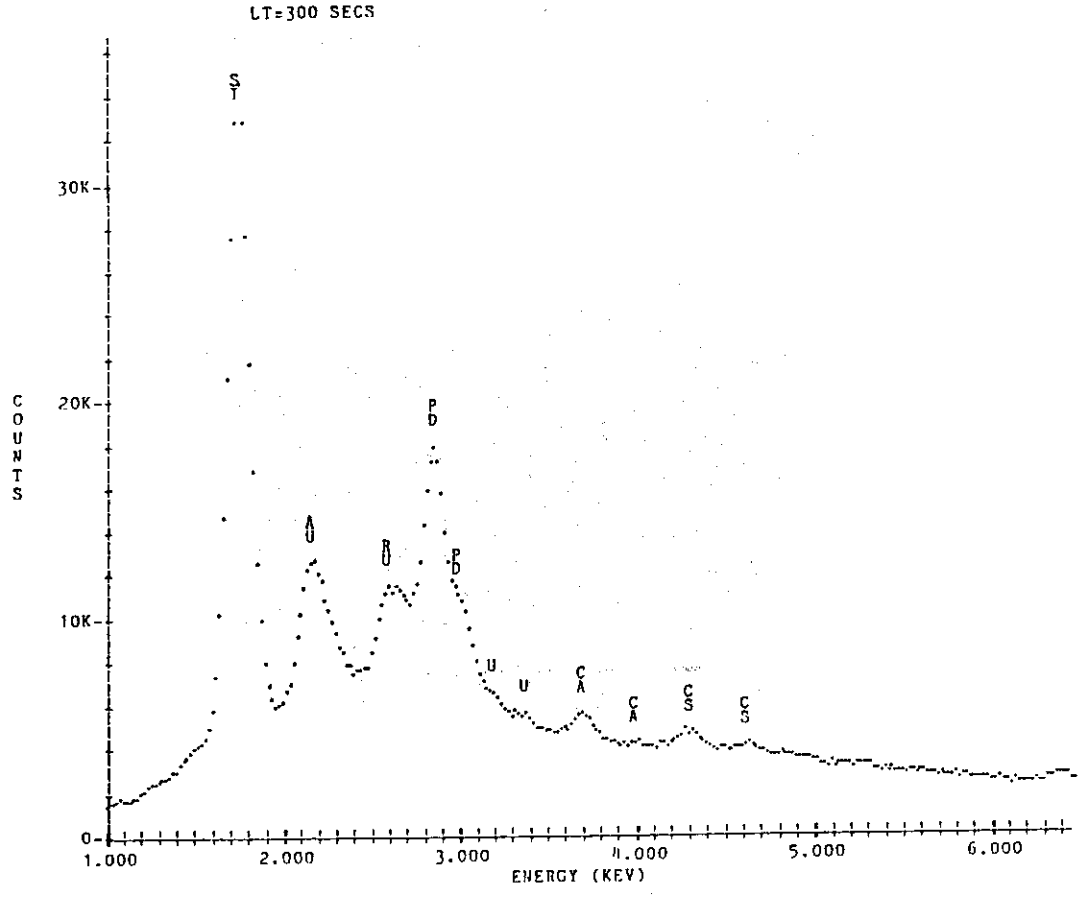

Fig. 3.8 Energy-dispersive X-ray analysis on the point 'A' marked in Fig. 3.6 (a).

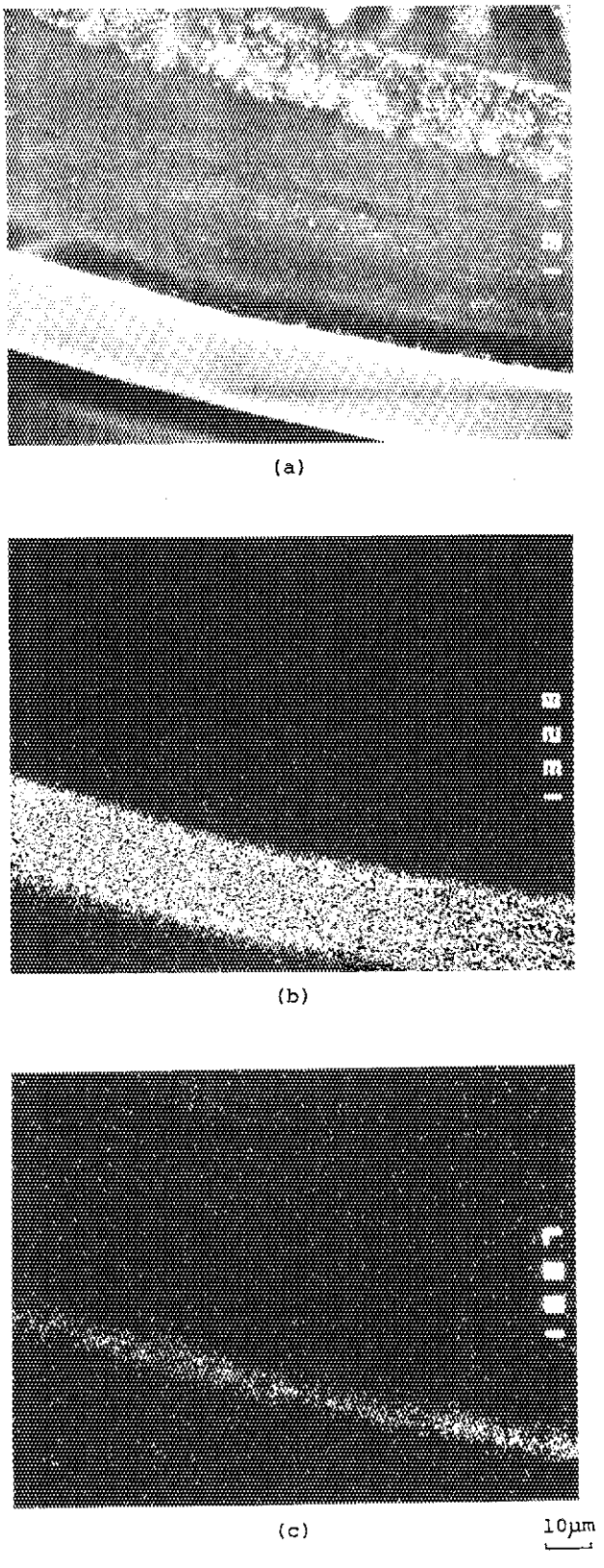

Fig. 3.9 Palladium accumulation at inner surface of the SiC layer on the cold side of 3A-3 particle irradiated in 73F-13A capsule. (a) Secondary electron image; (b) Si-Kα image; (c) Pd-Lα image.

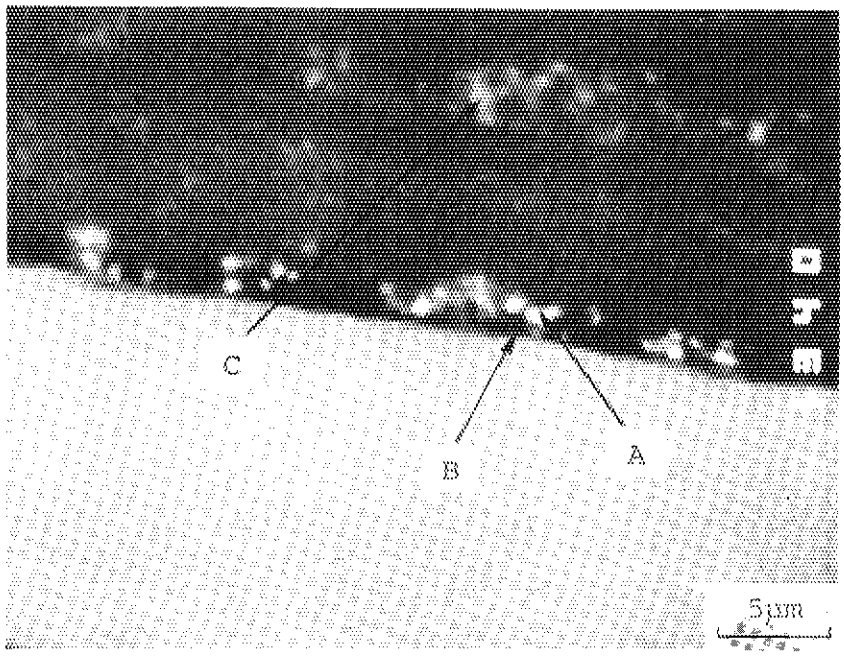

Fig. 3.10 Backscattered electron image of the coating layers on the cold side of 3A-3 particle irradiated in 73F-13A capsule. Letters indicate X-ray analyzed points.

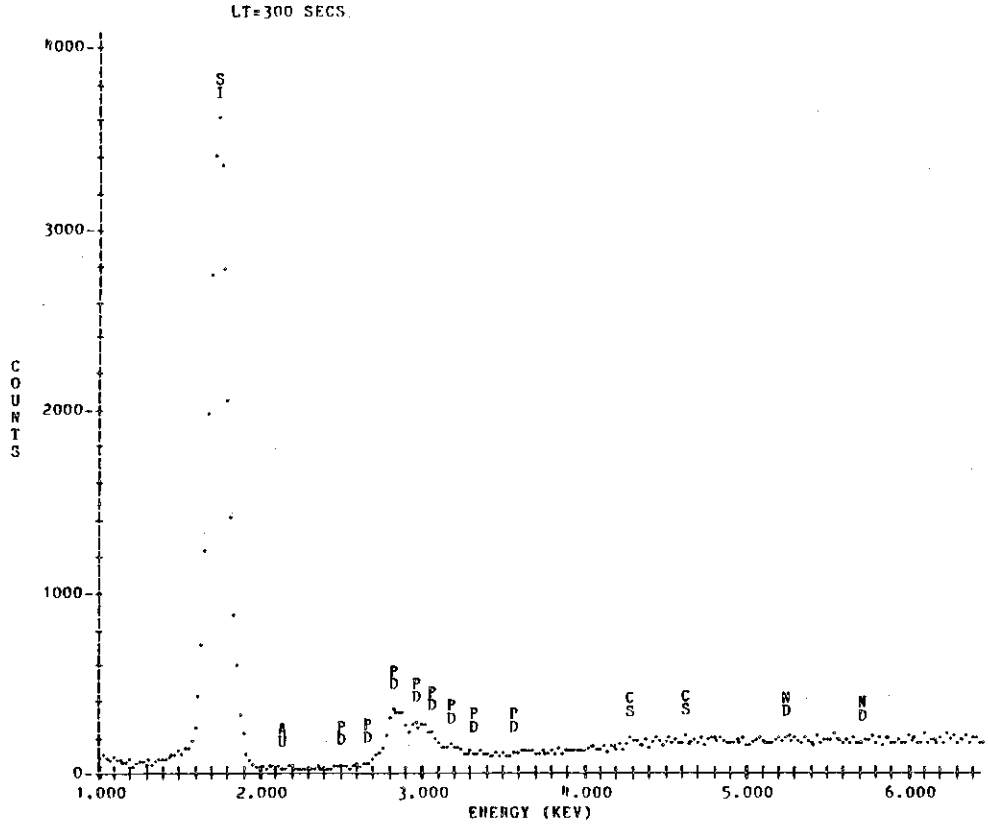

Fig. 3.11 (a) Energy-dispersive X-ray analysis on the point 'A' marked in Fig. 3.10.

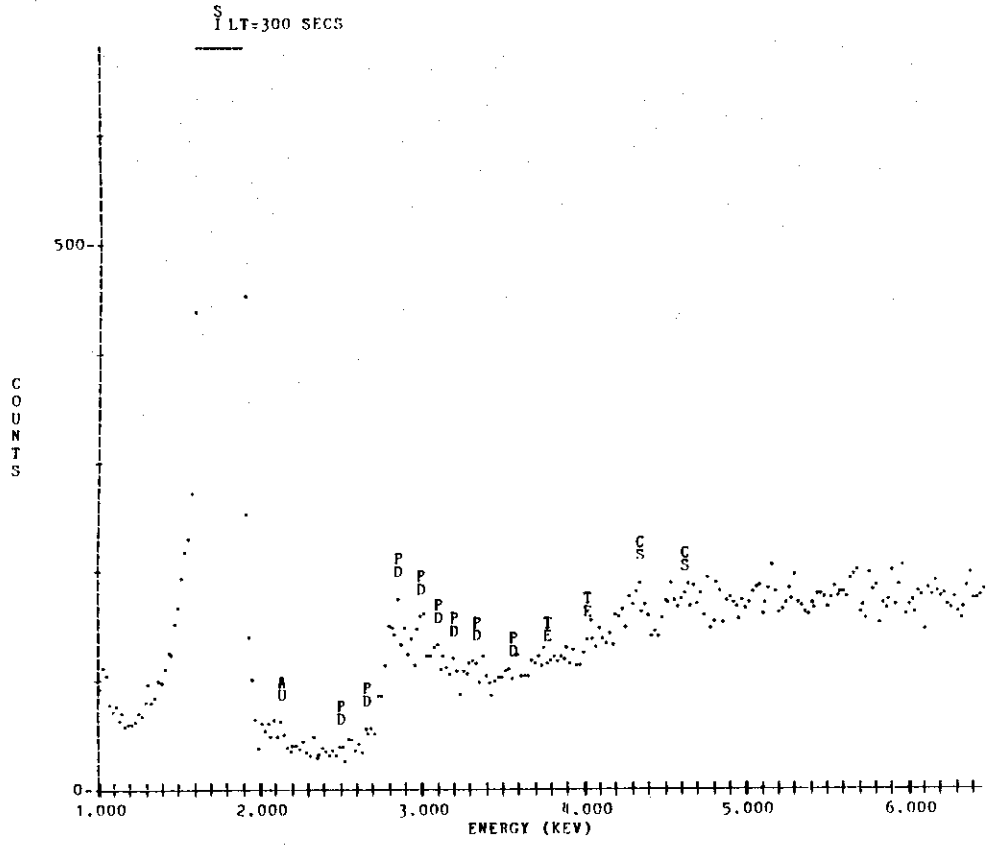

Fig. 3.11 (b) Energy-dispersive X-ray analysis on the point 'B' marked in Fig. 3.10.

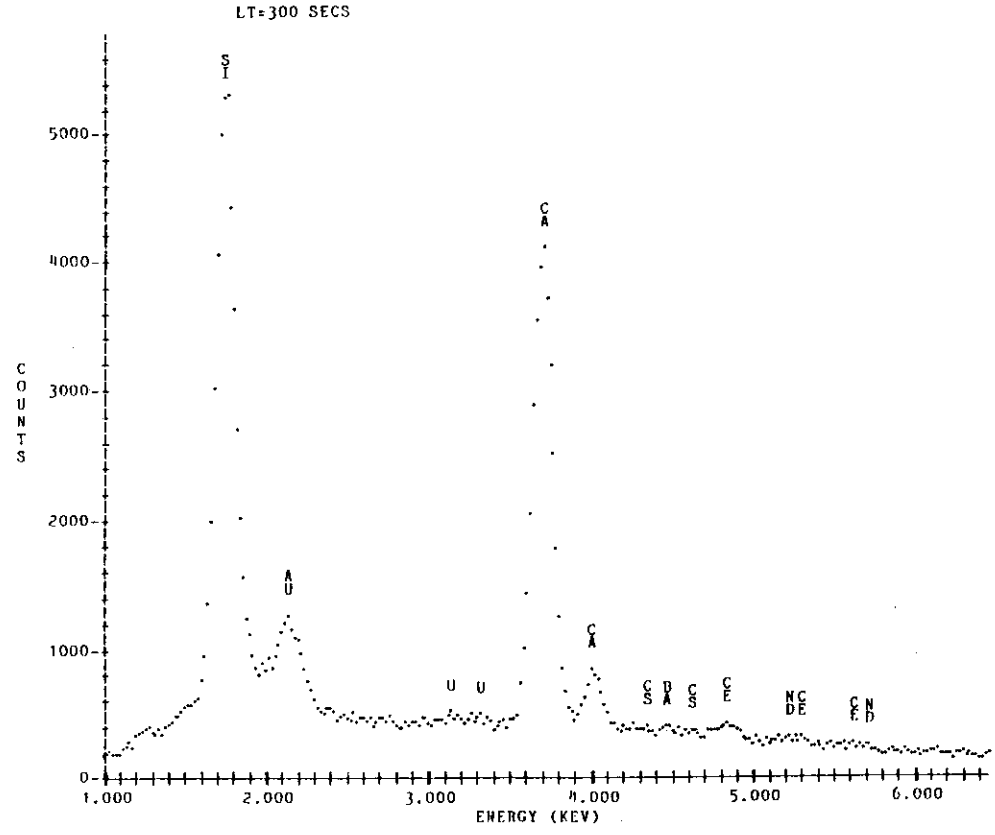

Fig. 3.11 (c) Energy-dispersive X-ray analysis on the point 'C' marked in Fig. 3.10.

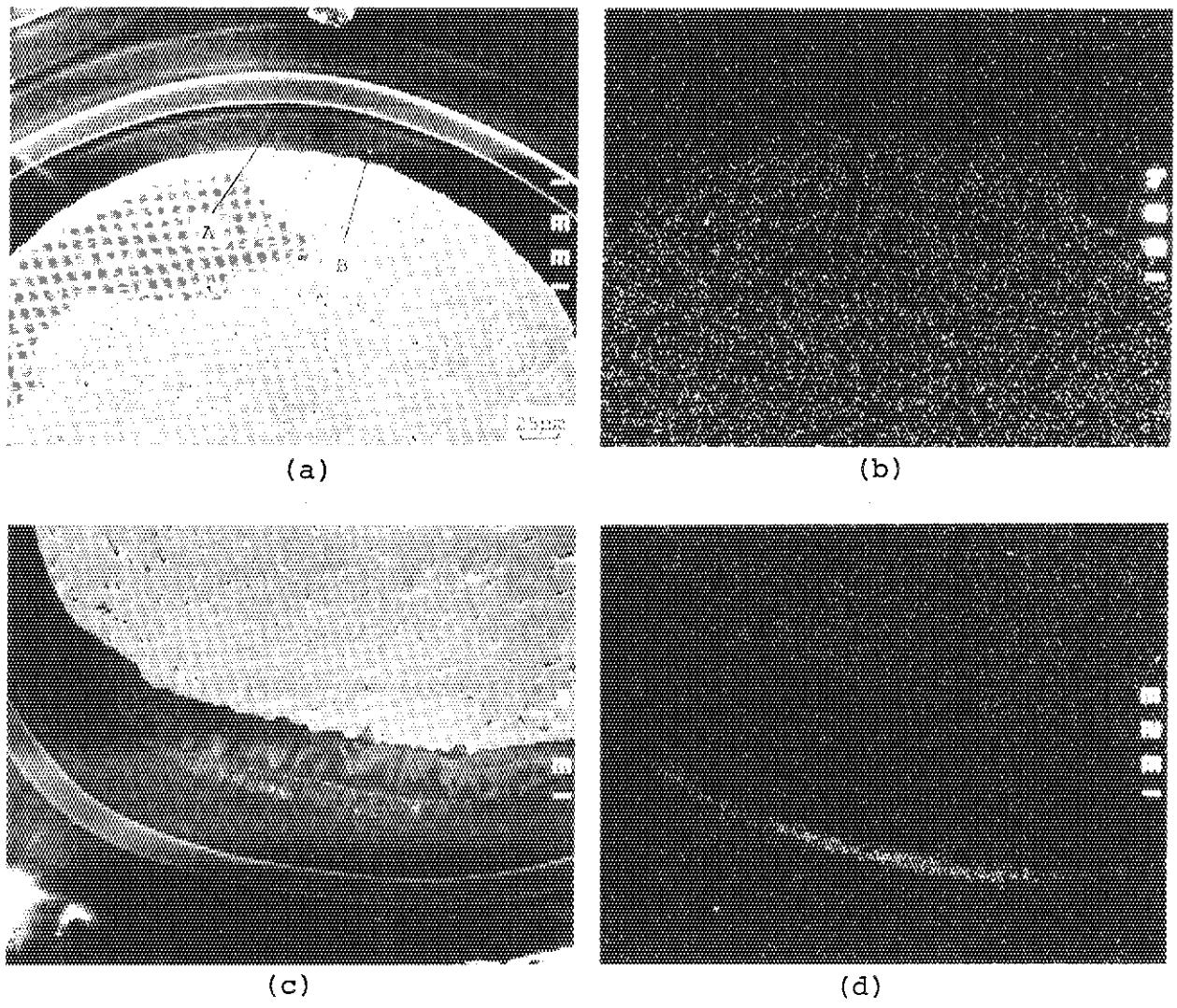

Fig. 3.12 Palladium accumulation at inner surface of the SiC layer of 3A-3 particle irradiated in 73F-13A capsule. Letters indicate X-ray analyzed points. (a) Secondary electron image of the hot side; (b) Pd-Lα image of the hot side; (c) Secondary electron image of the cold side; (d) Pd-Lα image of the cold side.

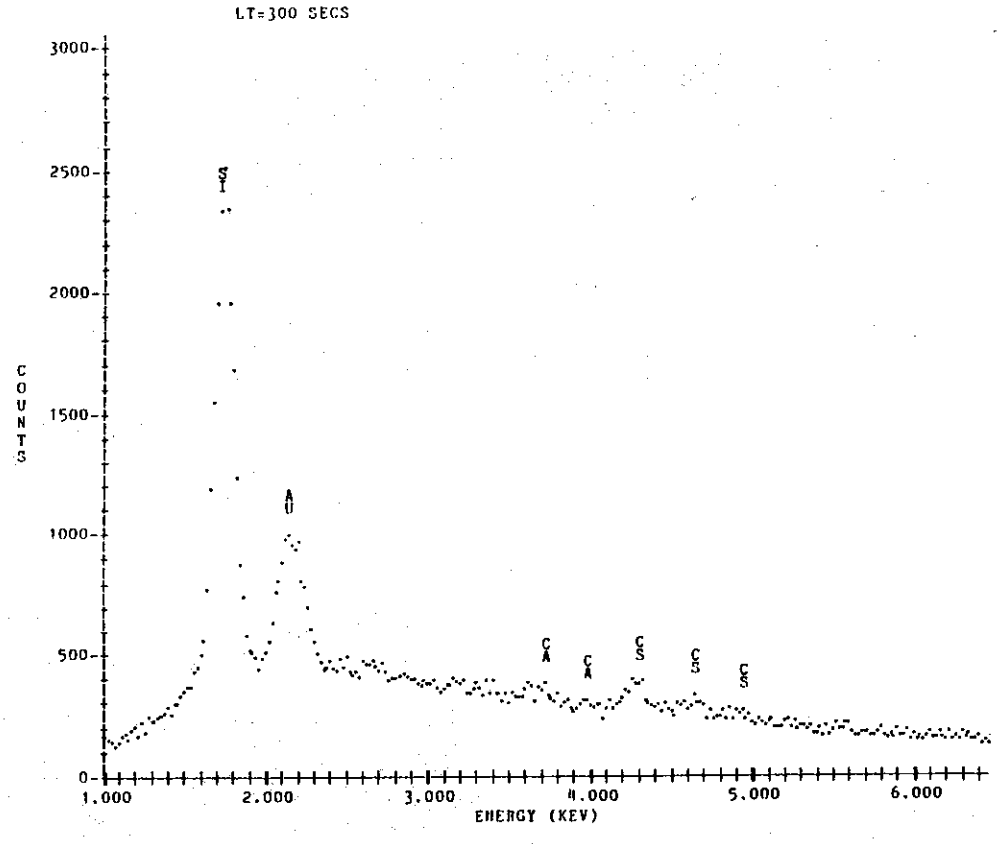

Fig. 3.13 (a) Energy-dispersive X-ray analysis on the point 'A' marked in Fig. 3.12 (a).

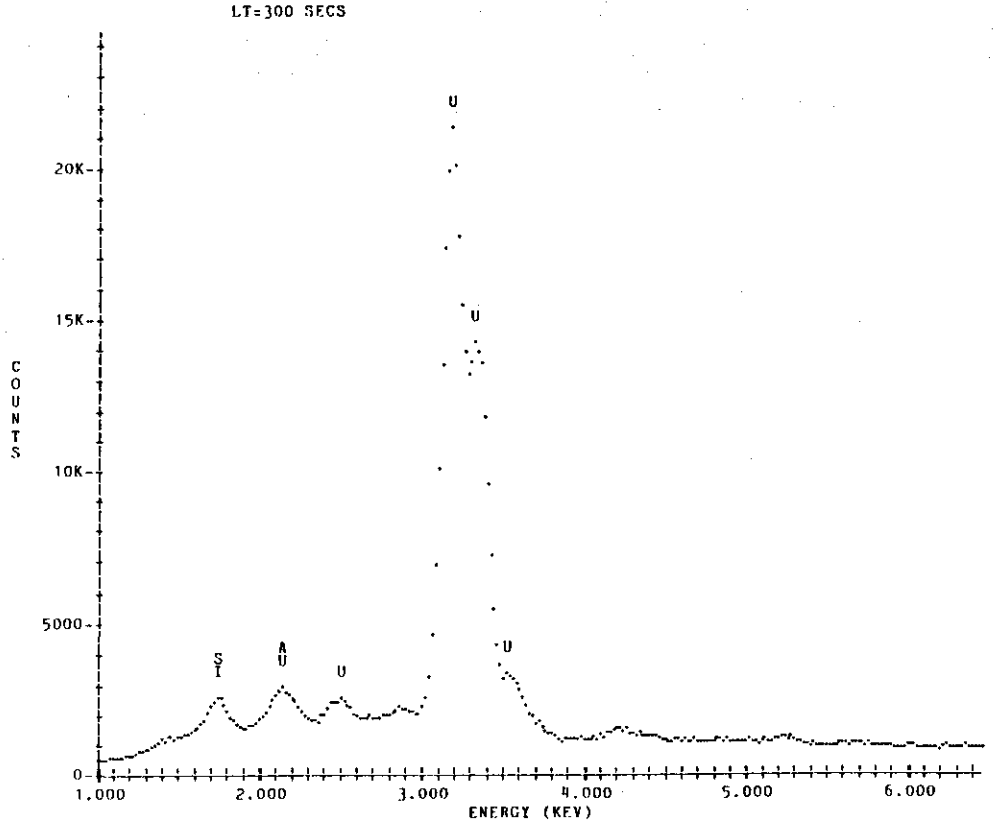

Fig. 3.13 (b) Energy-dispersive X-ray analysis on the point 'B' marked in Fig. 3.12 (a).

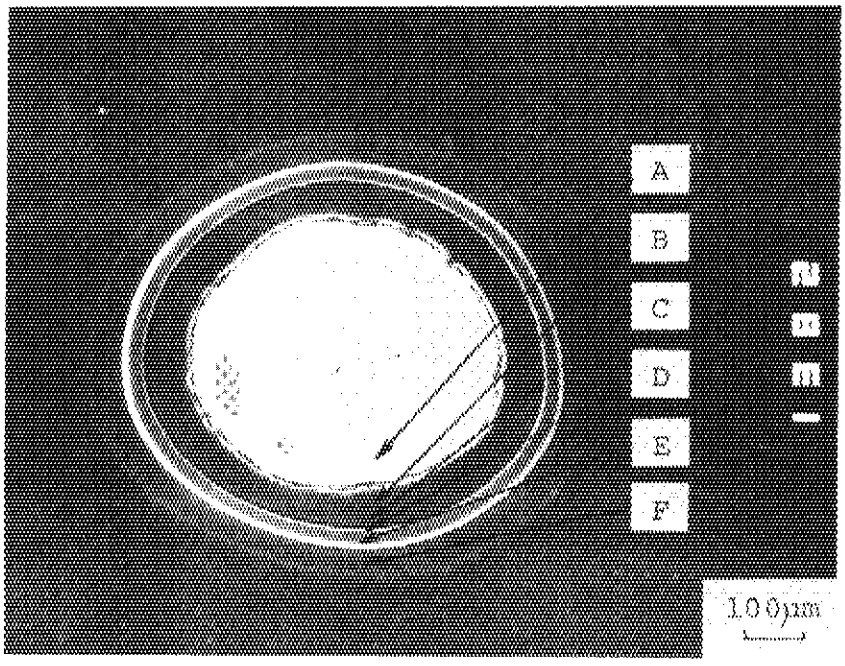

Fig. 3.14 Secondary electron image of 5A-1 particle irradiated in 73F-13A capsule. Letters indicate X-ray analyzed points.

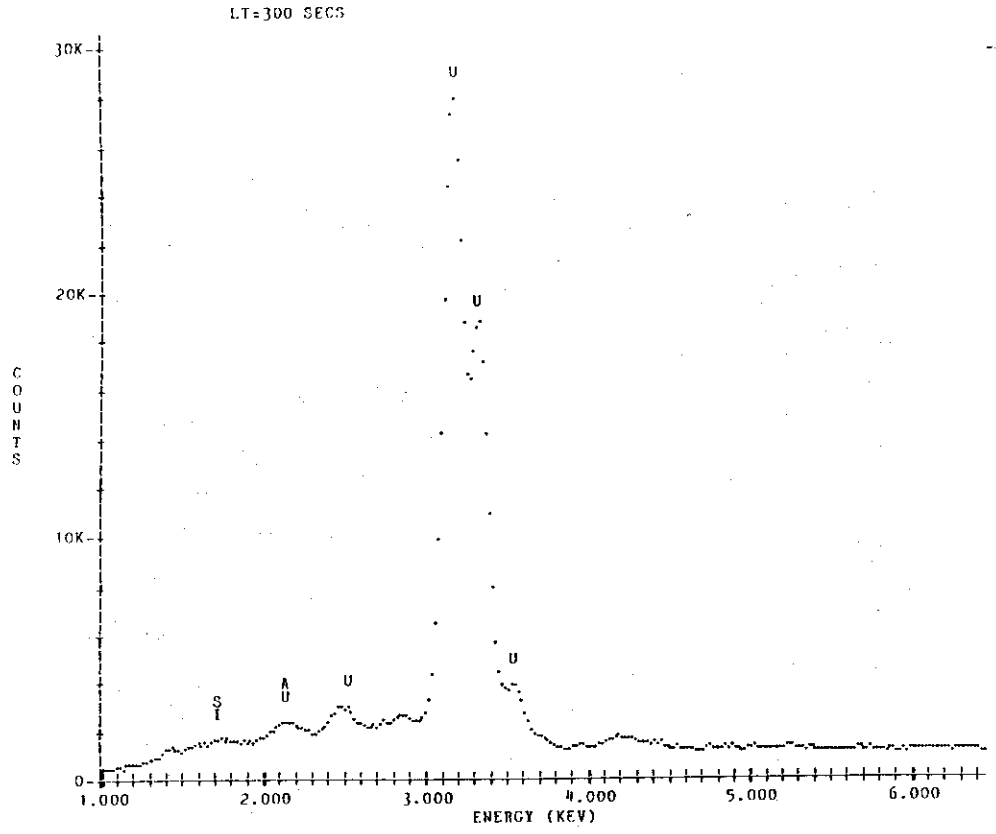

Fig. 3.15 (a) Energy-dispersive X-ray analysis on the point 'A' marked in Fig. 3.14.

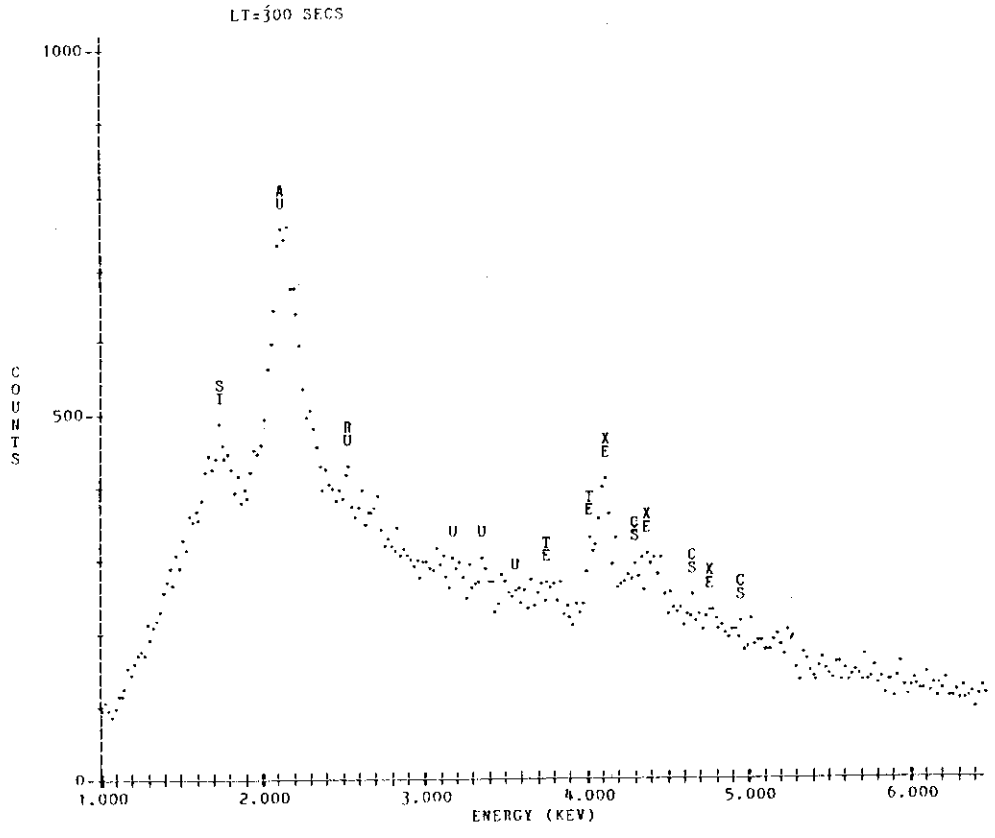

Fig. 3.15 (b) Energy-dispersive X-ray analysis on the point 'B' marked in Fig. 3.14.

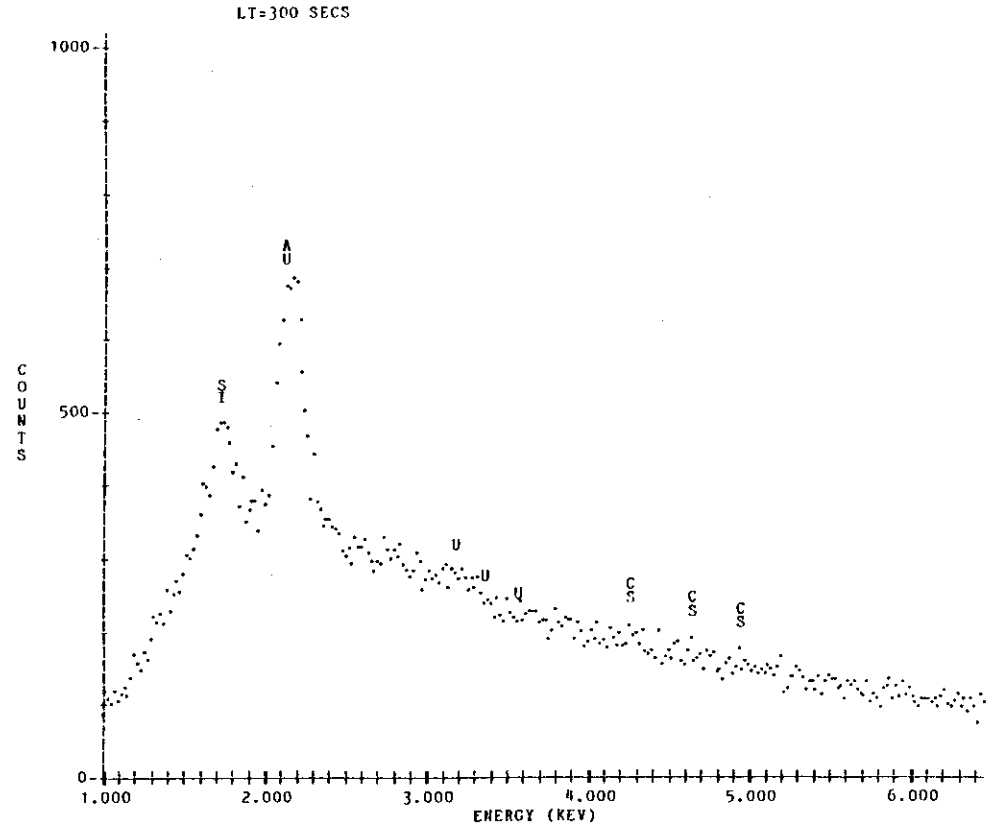

Fig. 3.15 (c) Energy-dispersive X-ray analysis on the point 'C' marked in Fig. 3.14.

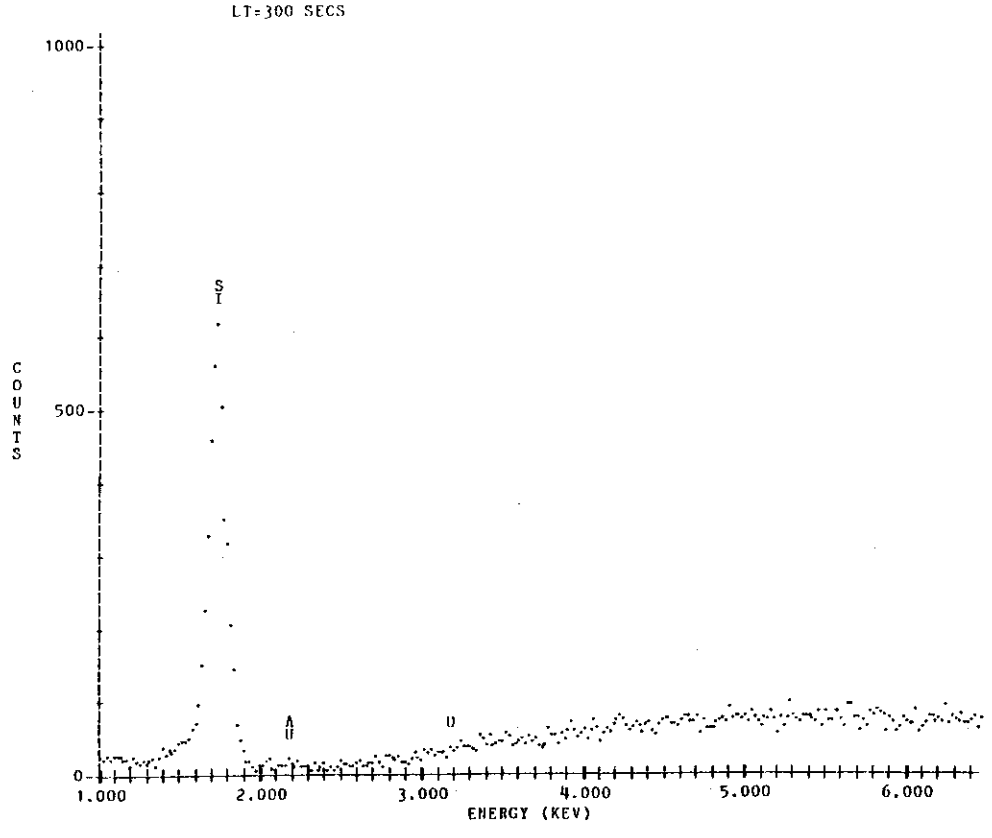

Fig. 3.15 (d) Energy-dispersive X-ray analysis on the point 'D' marked in Fig. 3.14.

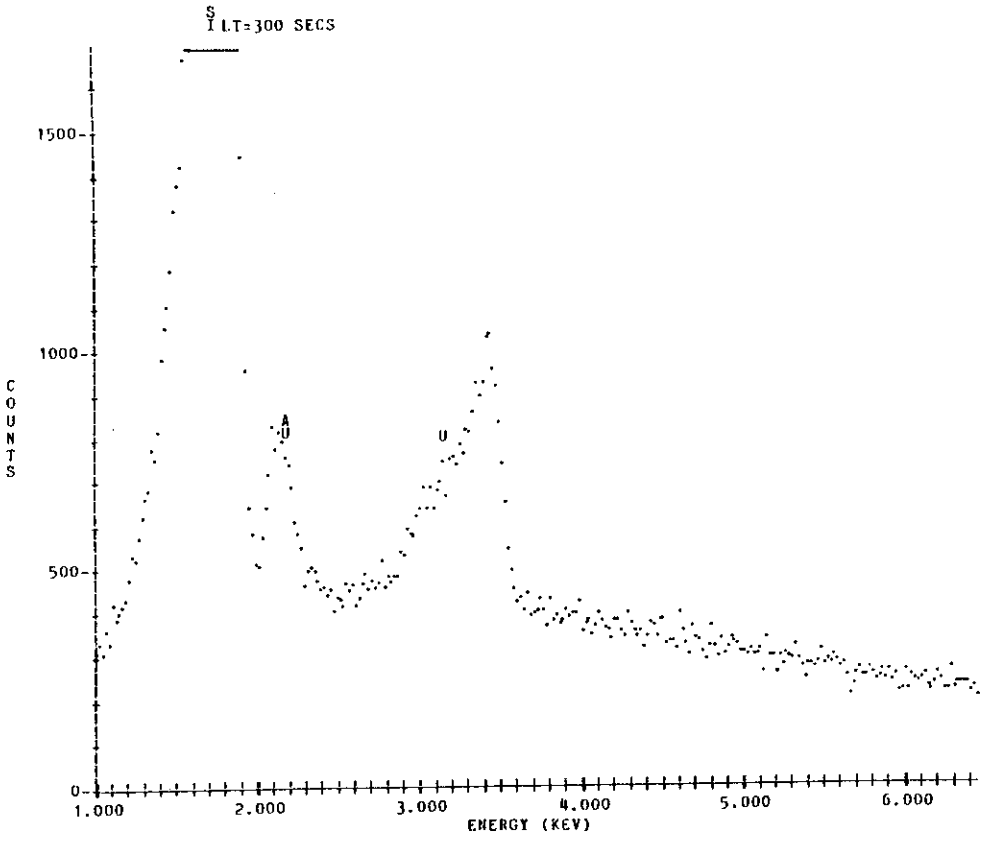

Fig. 3.15 (e) Energy-dispersive X-ray analysis on the point 'E' marked in Fig. 3.14.

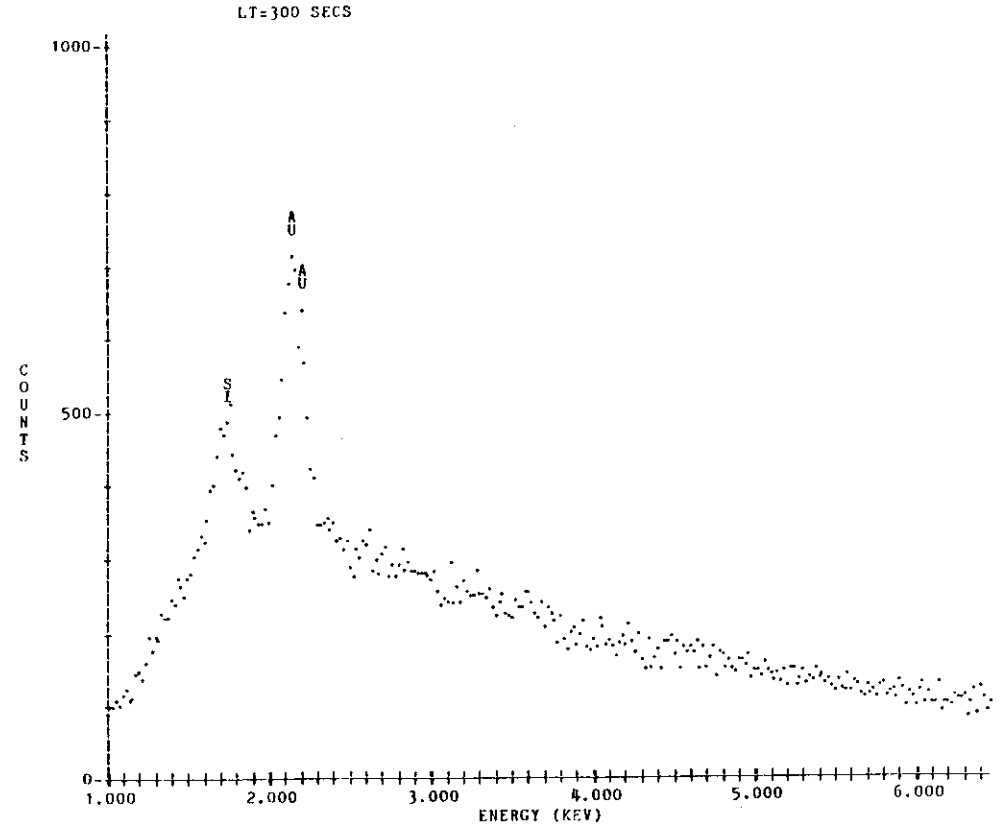

Fig. 3.15 (f) Energy-dispersive X-ray analysis on the point 'F' marked in Fig. 3.14.

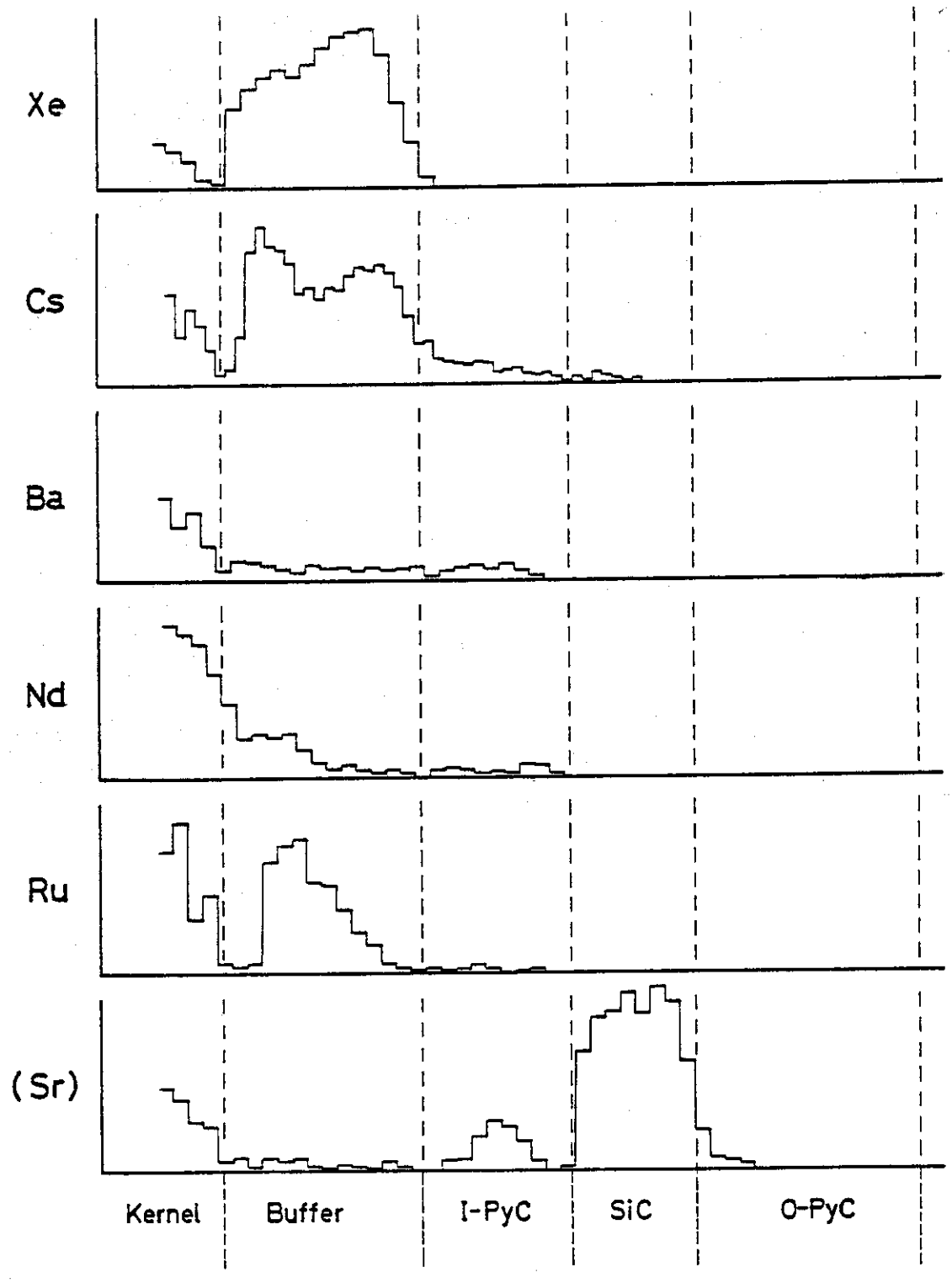

Fig. 3.16 Line scans across the coating layers of intact particles.

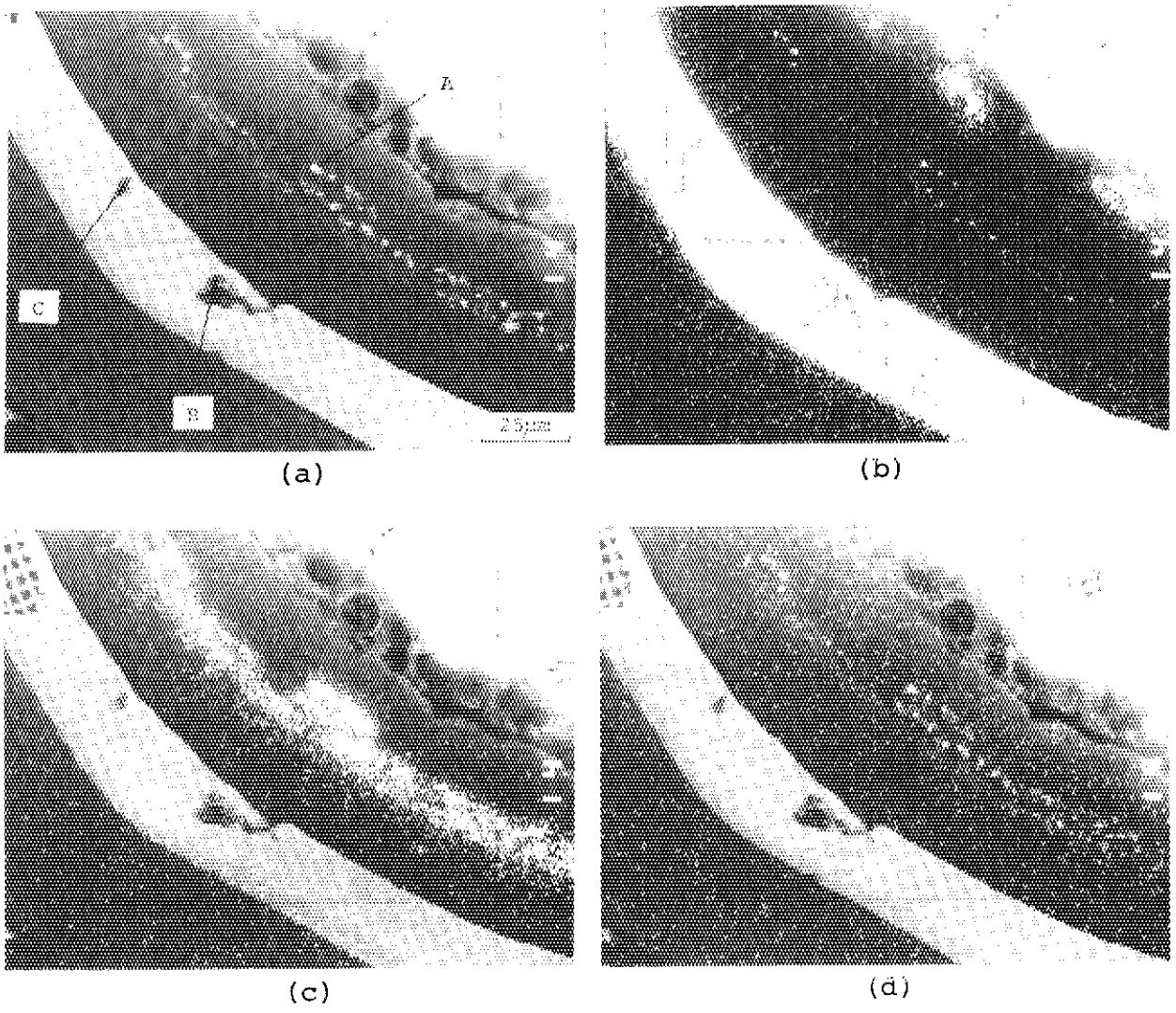

Fig. 3.17 Coating layers of 5B-1 particle irradiated in 73F-13A capsule. Letters indicate X-ray analyzed points. (a) Backscattered electron image(COMPO); (b) COMPO plus Si-Kα image; (c) COMPO plus Al-Kα image; (d) COMPO plus Ca-Kα image.

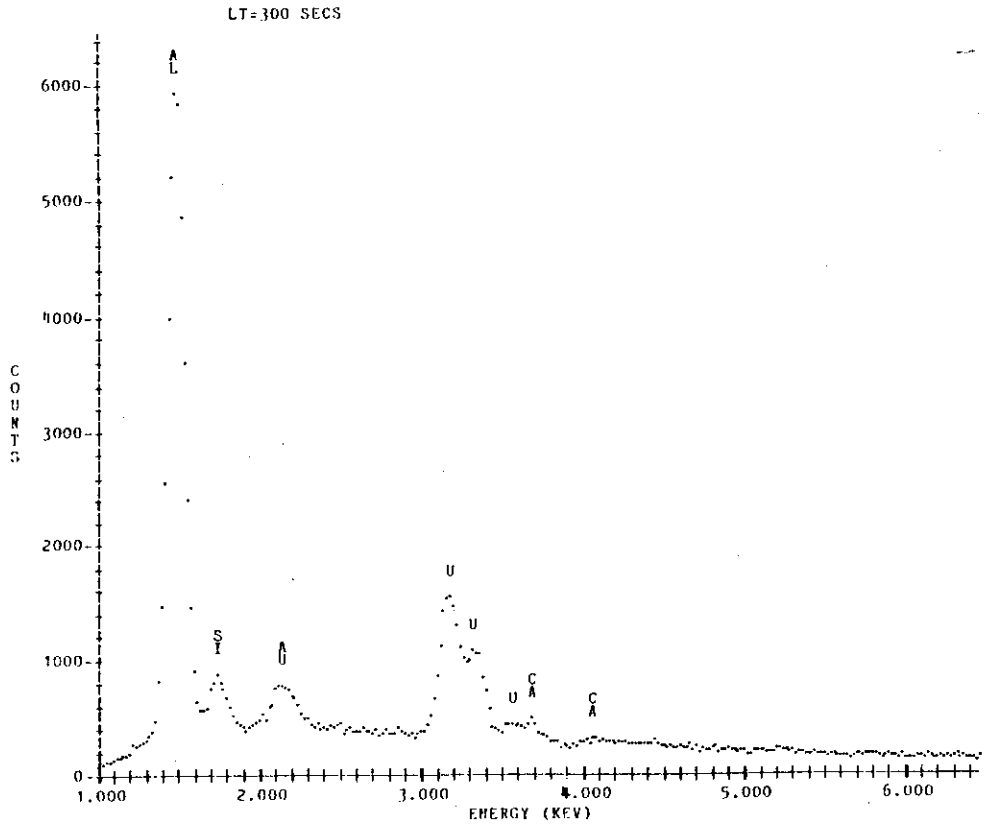

Fig. 3.18 (a) Energy-dispersive X-ray analysis on the point 'A' marked in Fig. 3.17 (a).

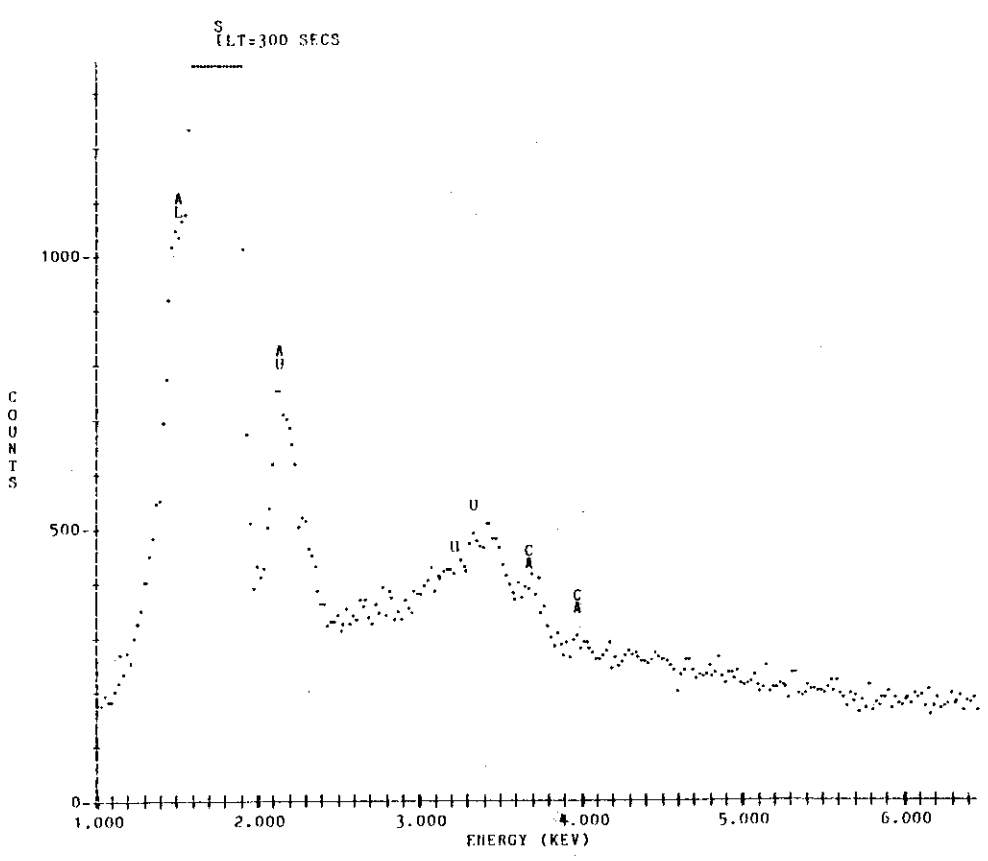

Fig. 3.18 (b) Energy-dispersive X-ray analysis on the point 'B' marked in Fig. 3.17 (a).

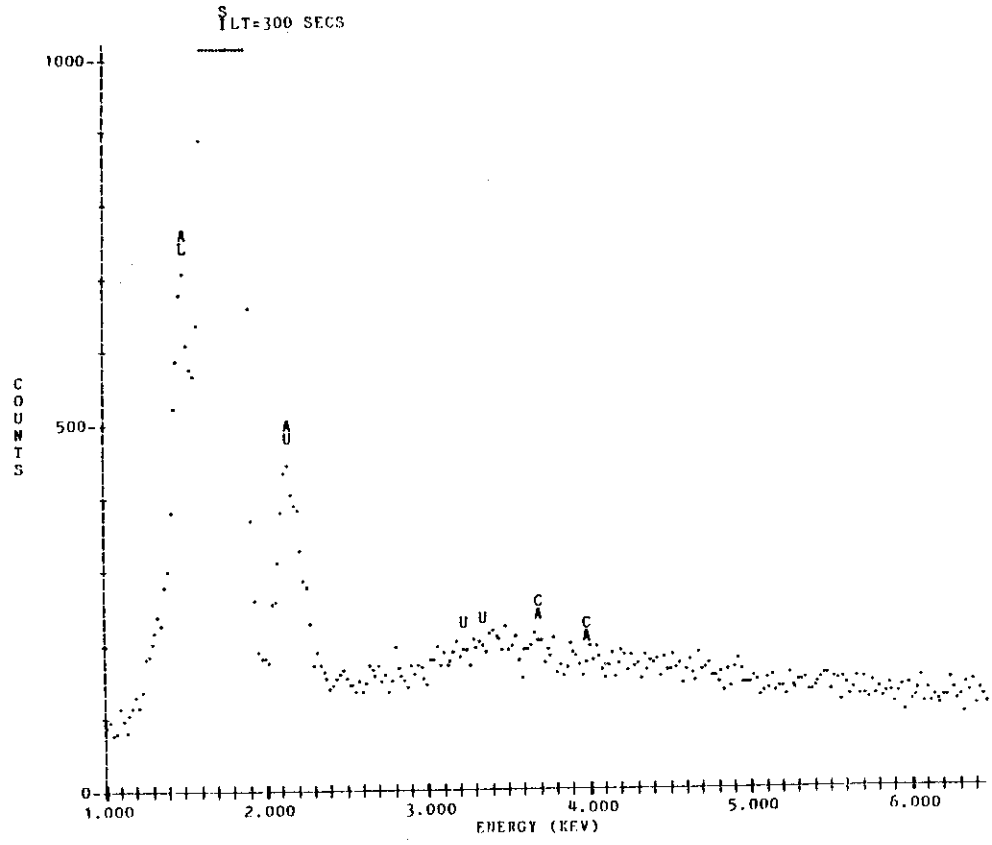

Fig. 3.18 (c) Energy-dispersive X-ray analysis on the point 'C' marked in Fig. 3.17 (a).

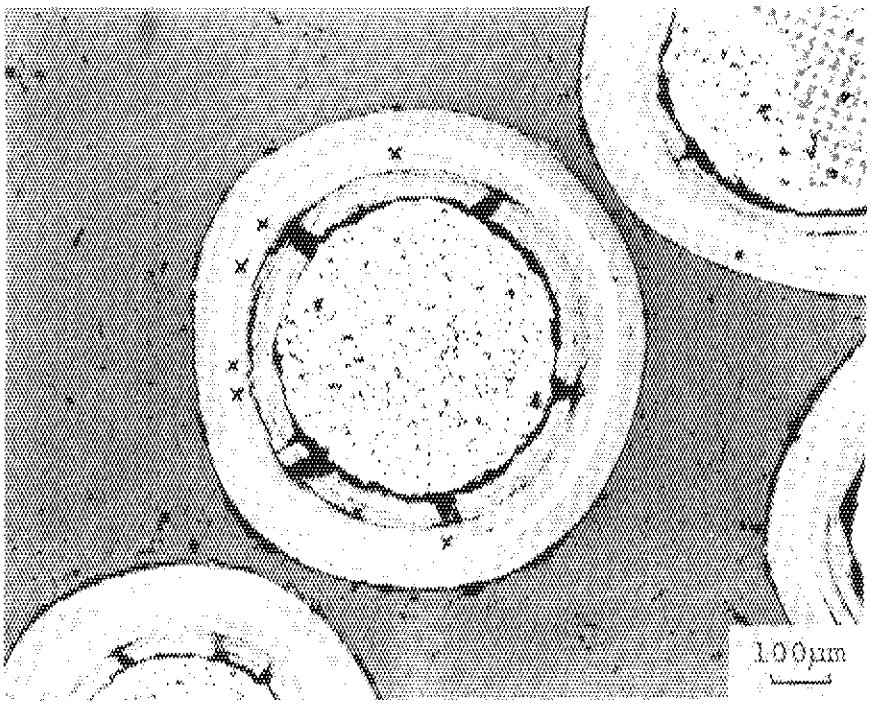

Fig. 3.19 Optical ceramograph of 75FP2A-1-1 particle irradiated in 75F-5A capsule. Symbol X indicates palladium accumulation positions.

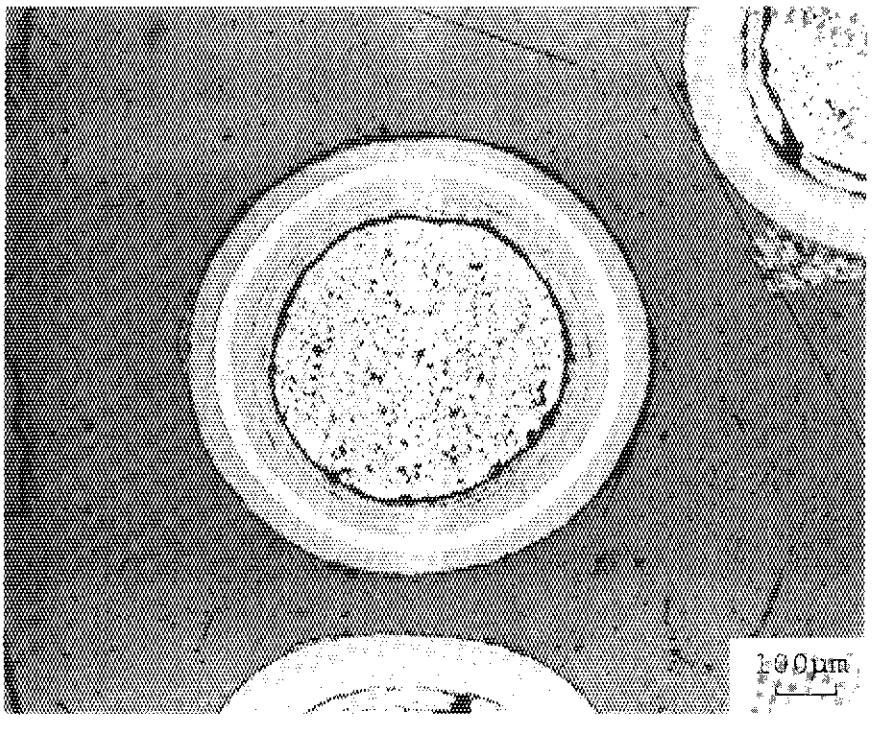

Fig. 3.20 Optical ceramograph of 75FP2A-1-2 particle irradiated in 75F-5A capsule.

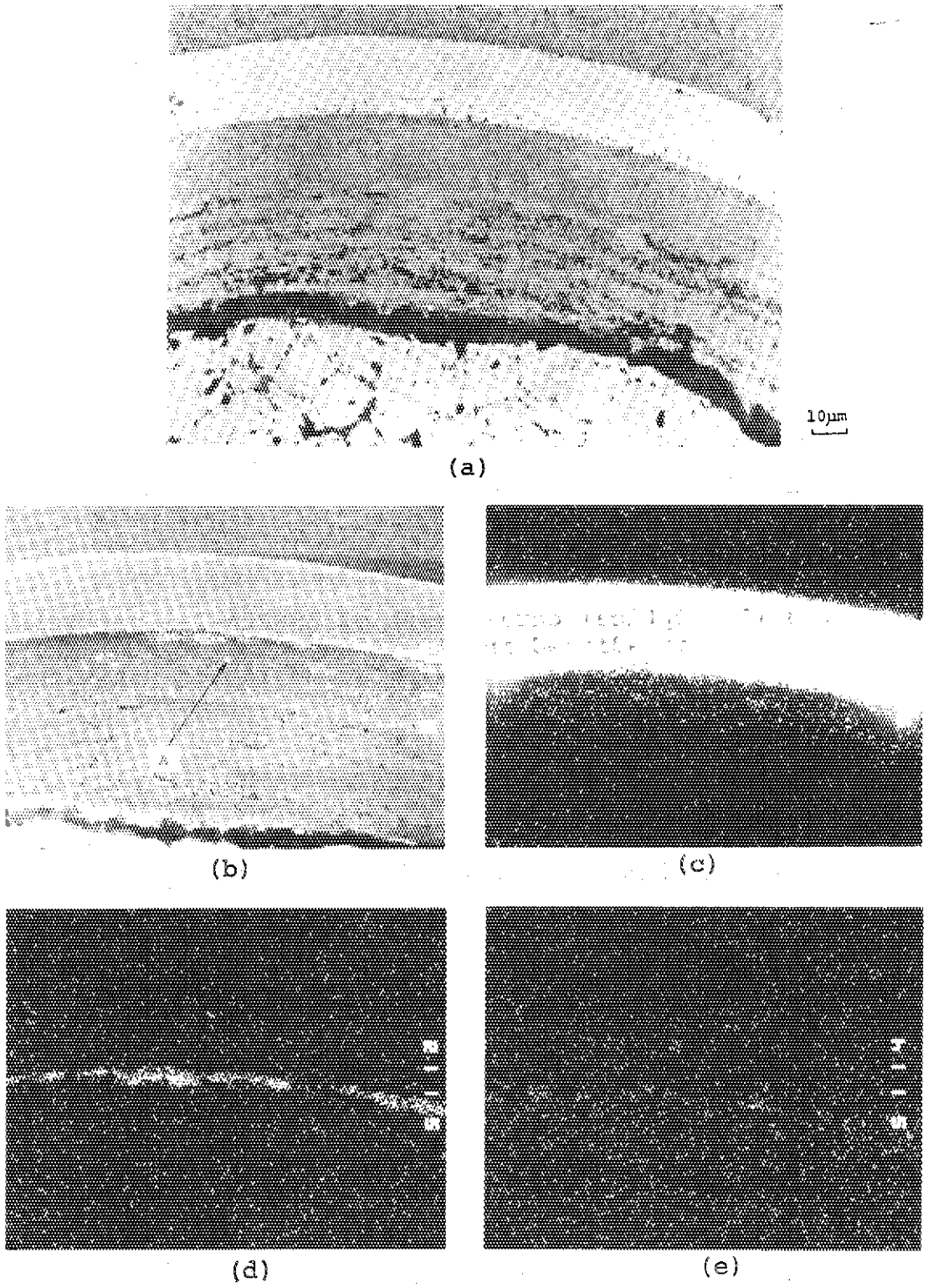

Fig. 3.21 Palladium accumulation at inner surface of 75FP2A-1-2 particle irradiated in 75F-5A capsule. Letter A indicates X-ray analyzed point. (a) Optical ceramograph; (b) Secondary electron image; (c) Si-Kα image; (d) Pd-Lα image; (e) Ba-Lα image.

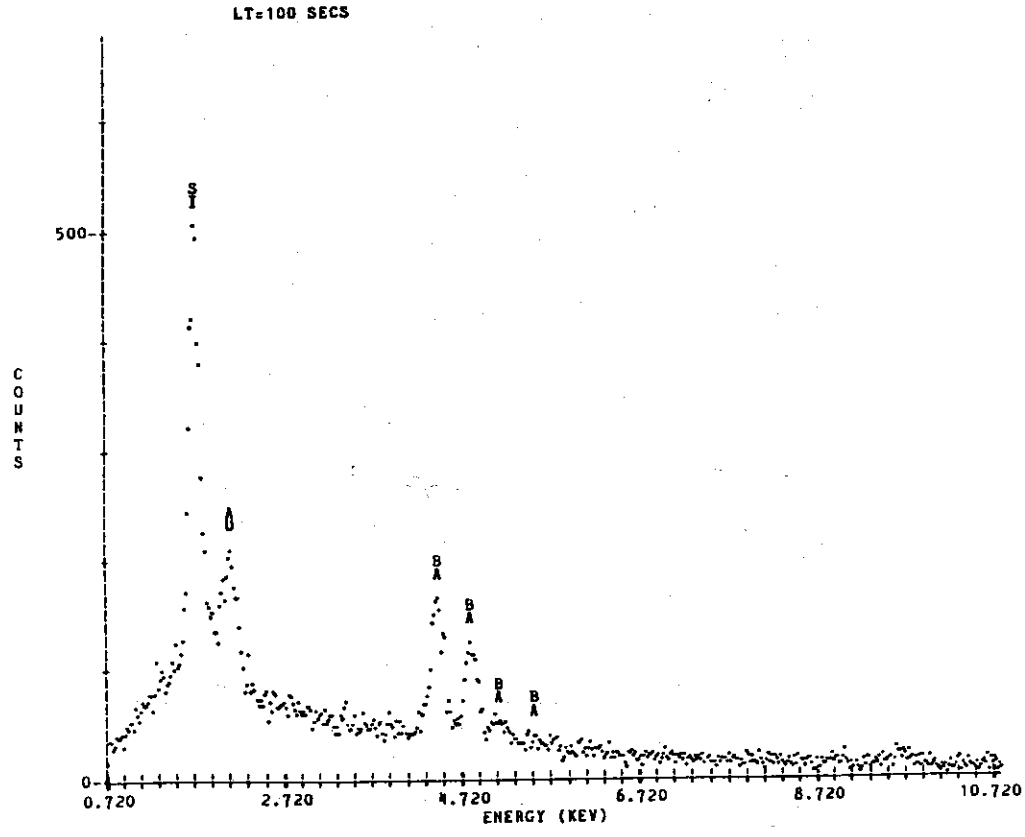

Fig.3.22 Energy-dispersive X-ray analysis on the point 'A' marked in Fig. 3.21 (b).

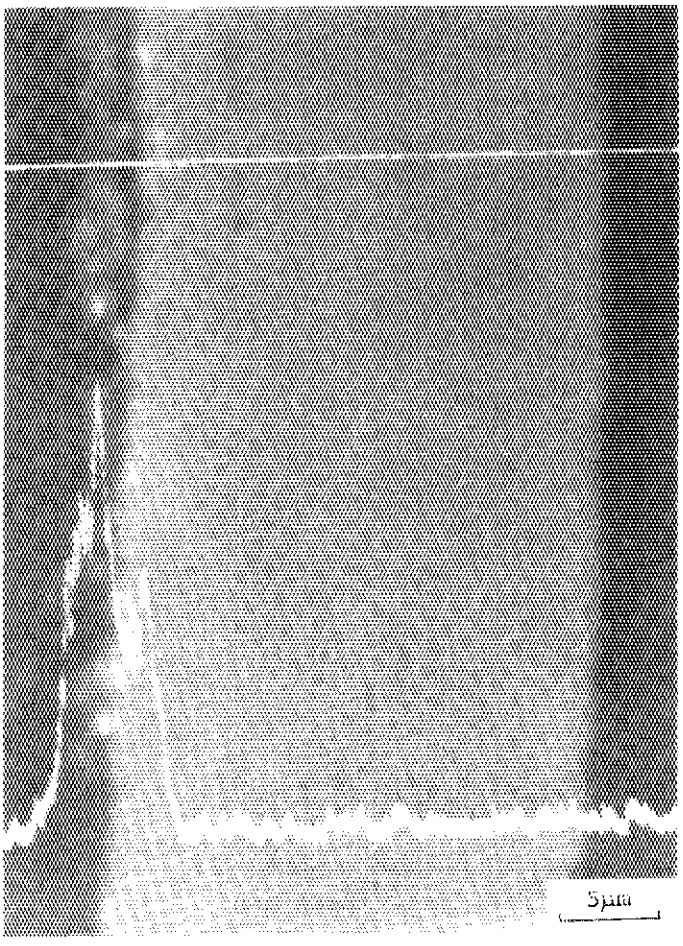

Fig. 3.23 Line scan for Pd-Lα X-ray across the coating layers of 75FP2A-1-2 particle irradiated in 75F-5A capsule.

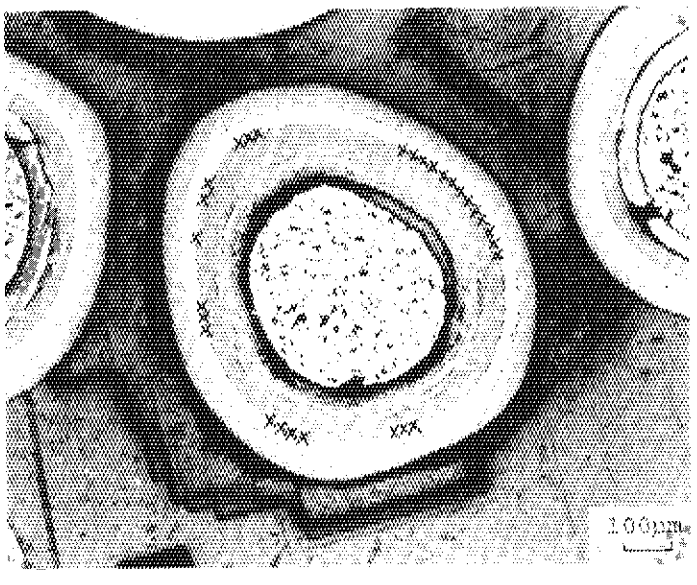

Fig. 3.24 Optical ceramograph of 760PC3-1 particle irradiated in 75F-4A capsule. Symbol X indicates palladium accumulation positions.

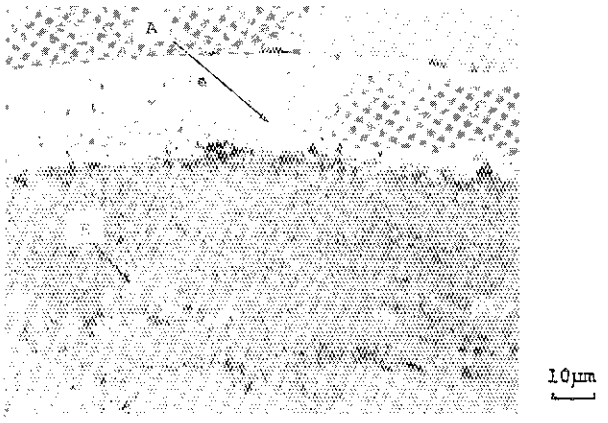

(a)

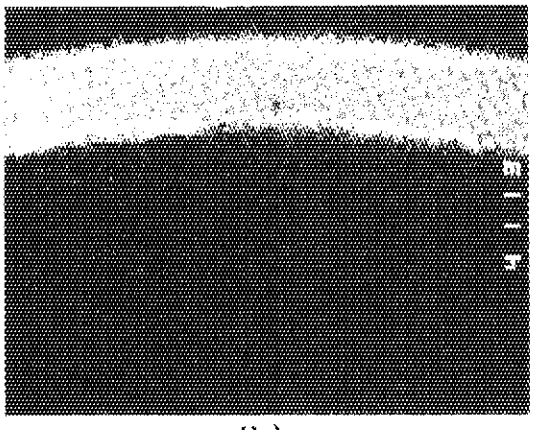

(b)

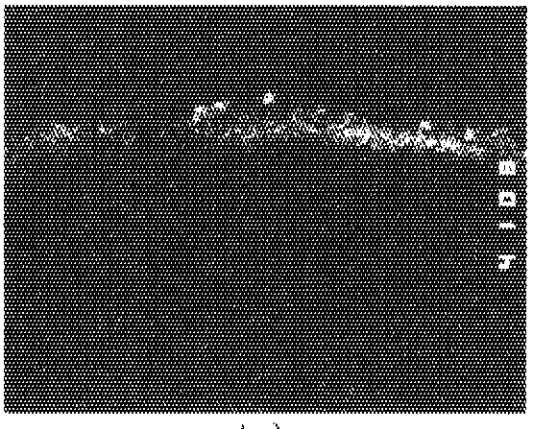

(c)

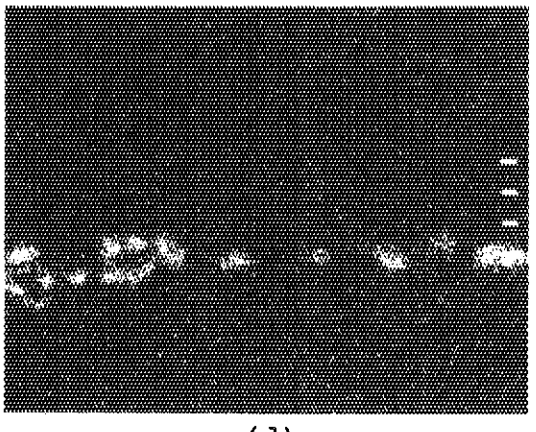

(d)

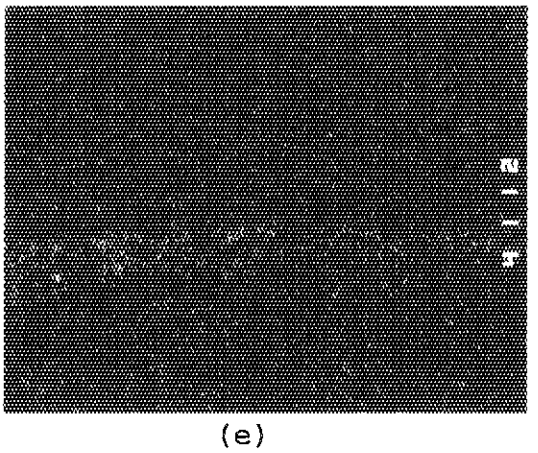

(e)

Fig. 3.25 Palladium penetration into the SiC layer on the cold side of 76OPC3-1 particle irradiated in 75F-4A capsule. Letters indicate X-ray analyzed points. (a) Optical ceramograph; (b) Si-Kα image; (c) Pd-Lα image; (d) Te-Lα image; (e) Ce-Lα image.

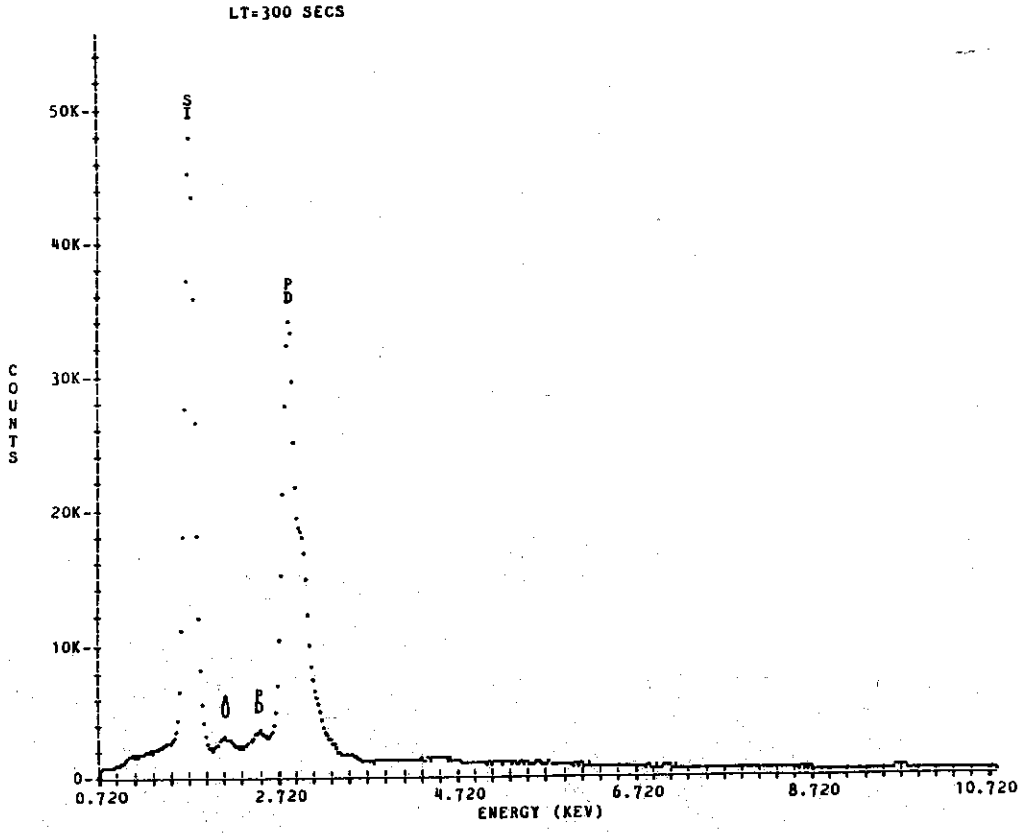

Fig. 3.26 (a) Energy-dispersive X-ray analysis on the point 'A' marked in Fig. 3.25 (a).

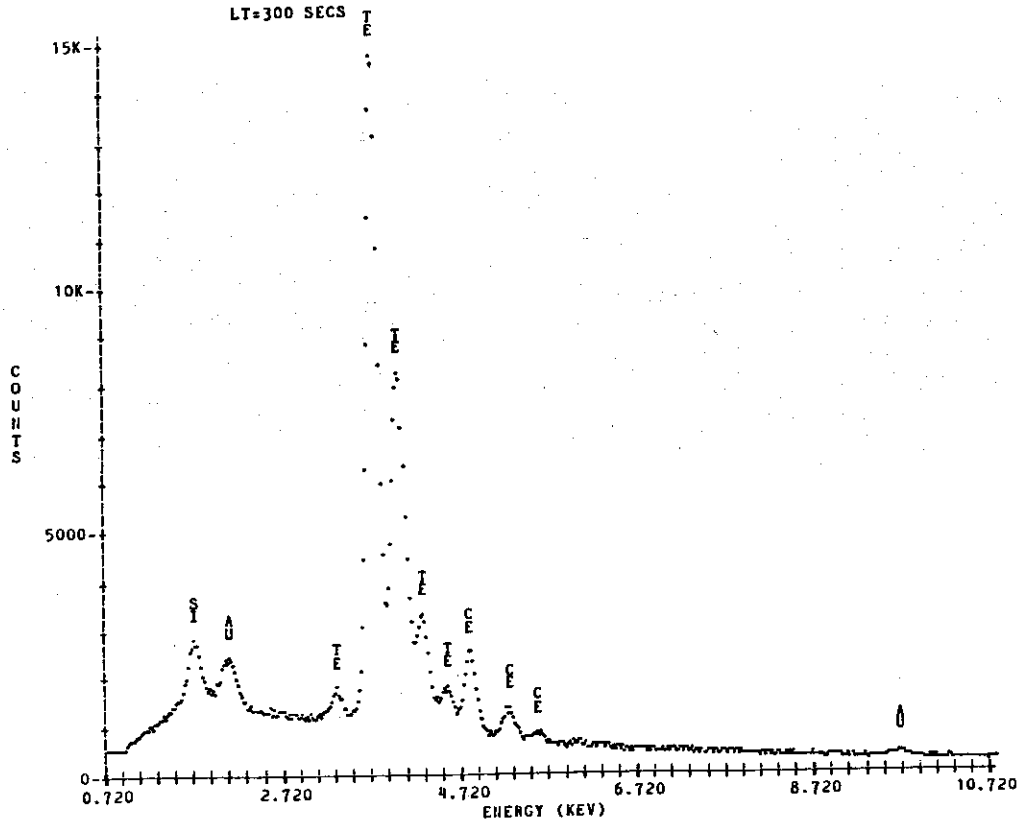

Fig. 3.26 (b) Energy-dispersive X-ray analysis on the point 'B' marked in Fig. 3.25 (a).

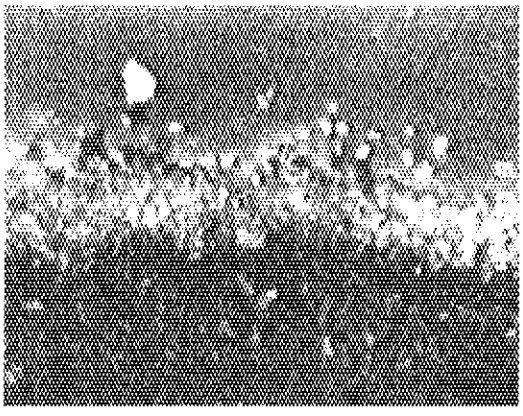

(a)

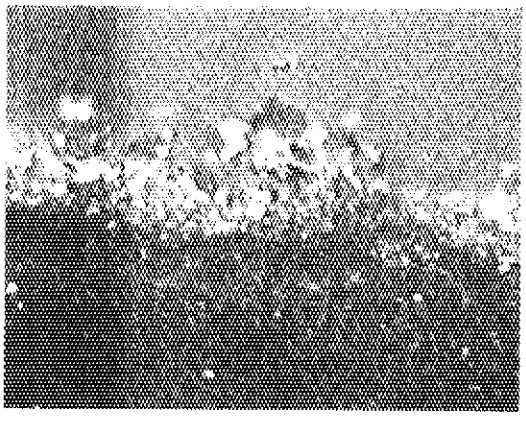

(b)

Fig. 3.27 Secondary electron images of Pd-SiC interaction area of 76OPC3-1 particle irradiated in 75F-4A capsule.

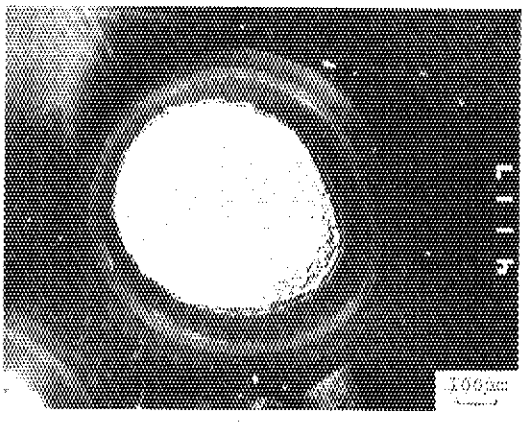

Fig. 3.28 Secondary electron image of 76OPC3-2 particle irradiated in 75F-4A capsule.

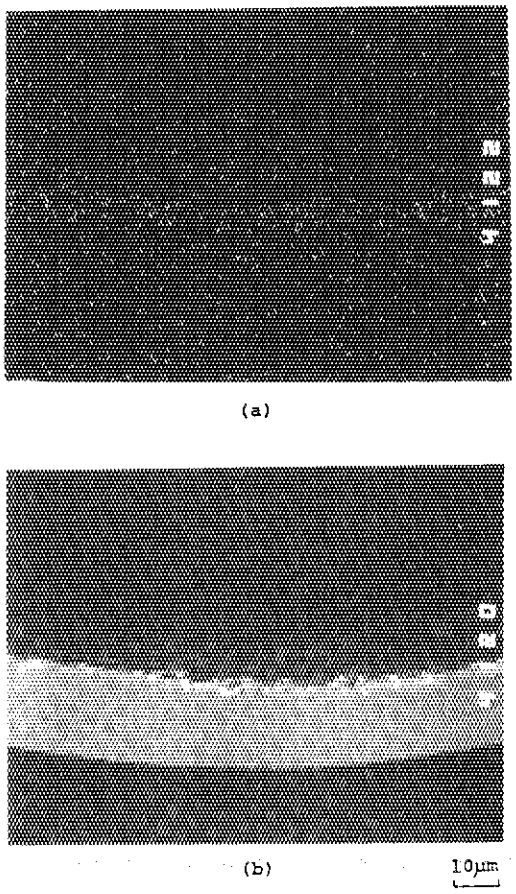

Fig. 3.29 Palladium accumulation at inner surface of the SiC layer on the cold side of 76OPC3-2 particle irradiated in 75F-4A capsule. (a) Backscattered electron image; (b) Pd-Lα image.

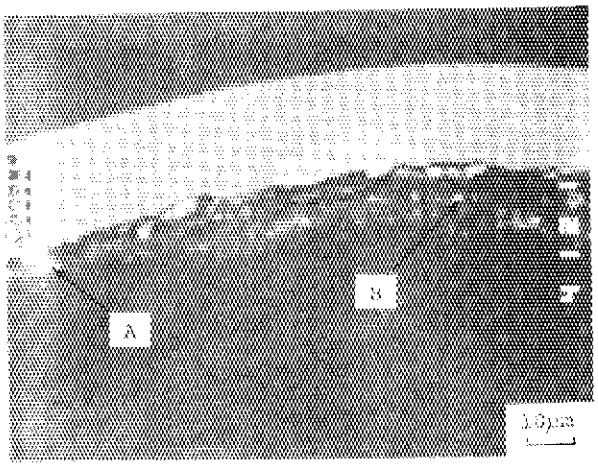

Fig. 3.30 White precipitates near the SiC layer of 76OPC3-2 particle irradiated in 75F-4A capsule. Letters indicate X-ray analyzed points.

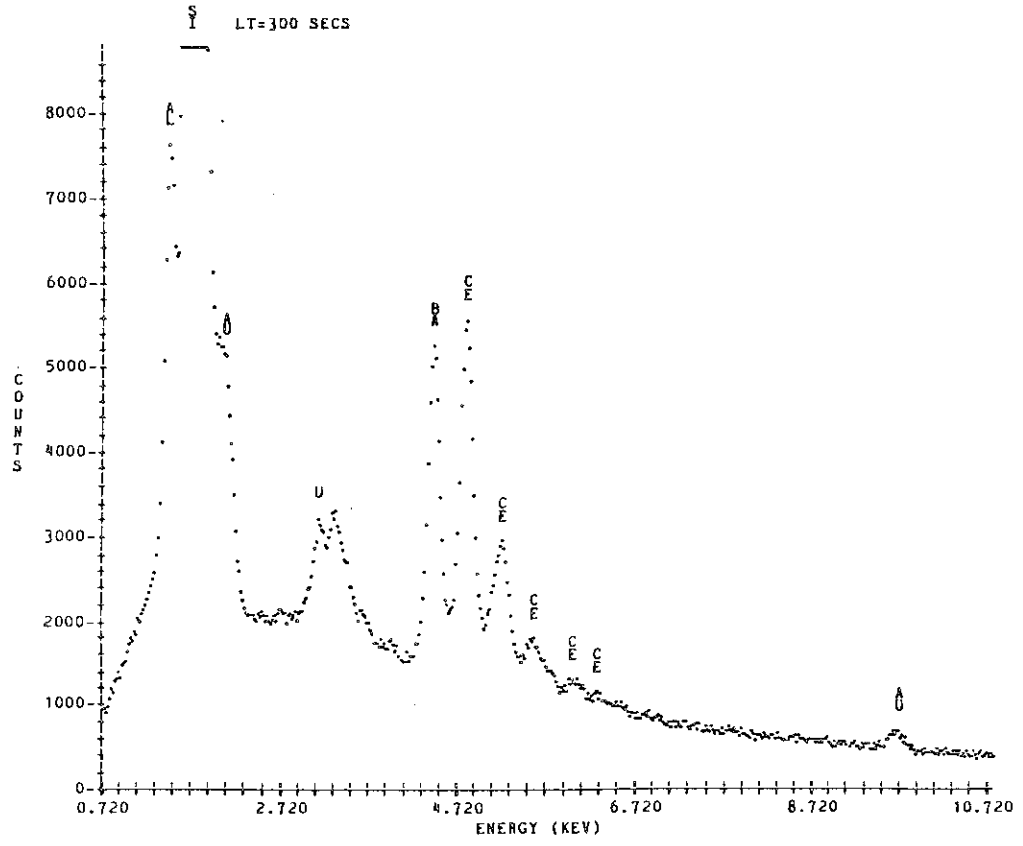

Fig. 3.31 (a) Energy-dispersive X-ray analysis on the point 'A' marked in Fig. 3.30.

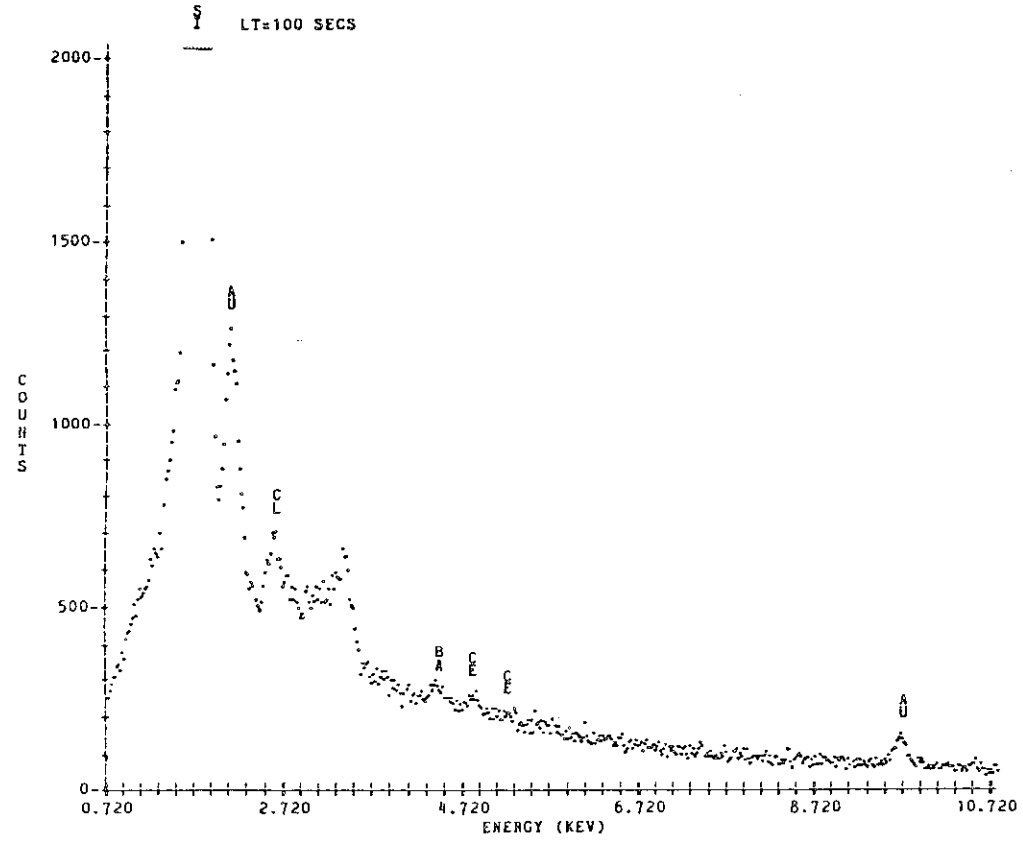

Fig. 3.31 (b) Energy dispersive X-ray analysis on the point 'B' marked in Fig. 3.30.

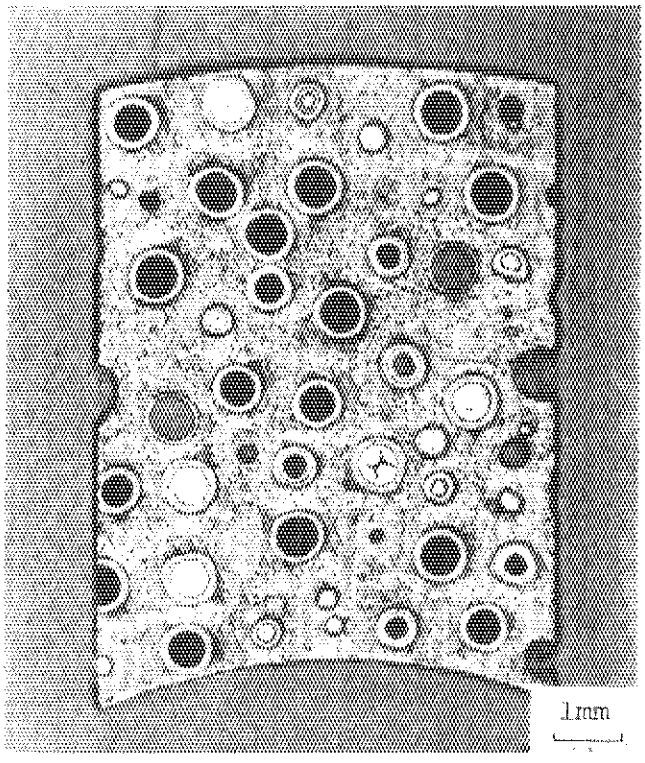

(a)

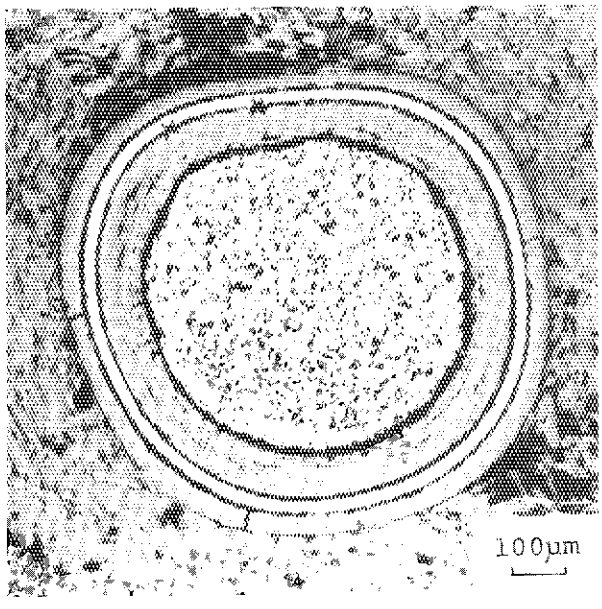

(b)

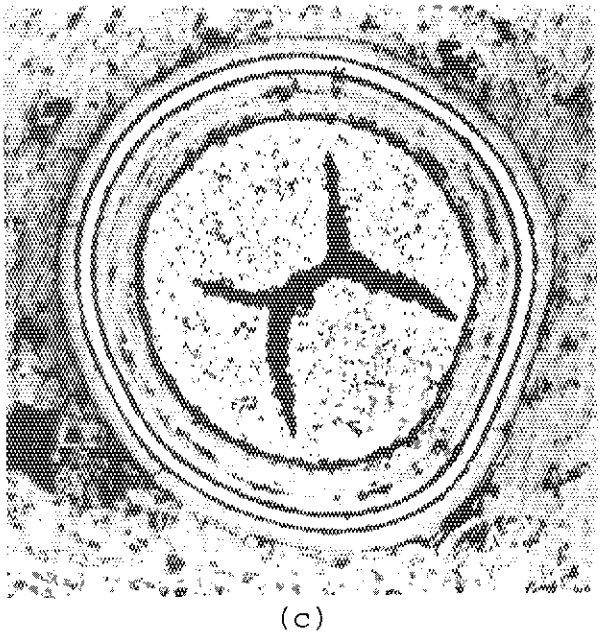

(c)

Fig. 3.32 Optical ceramographs of 76FP1A-9 compact irradiated in 77F-4A capsule. Symbol X indicates palladium accumulation positions. (a) Piece of 76FP1A-9 compact; (b) 76FP1A-9-1 particle; (c) 76FP1A-9-2 particle.

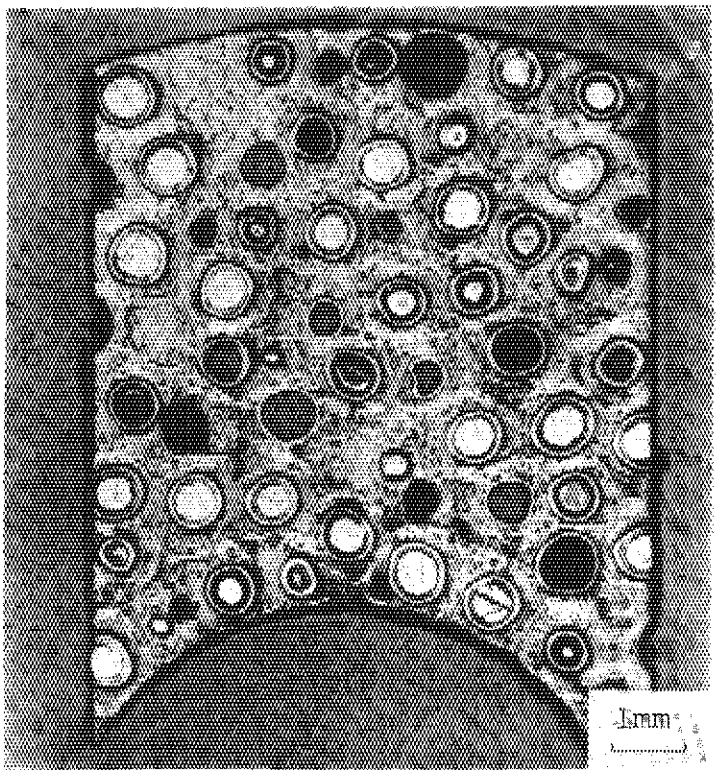

(a)

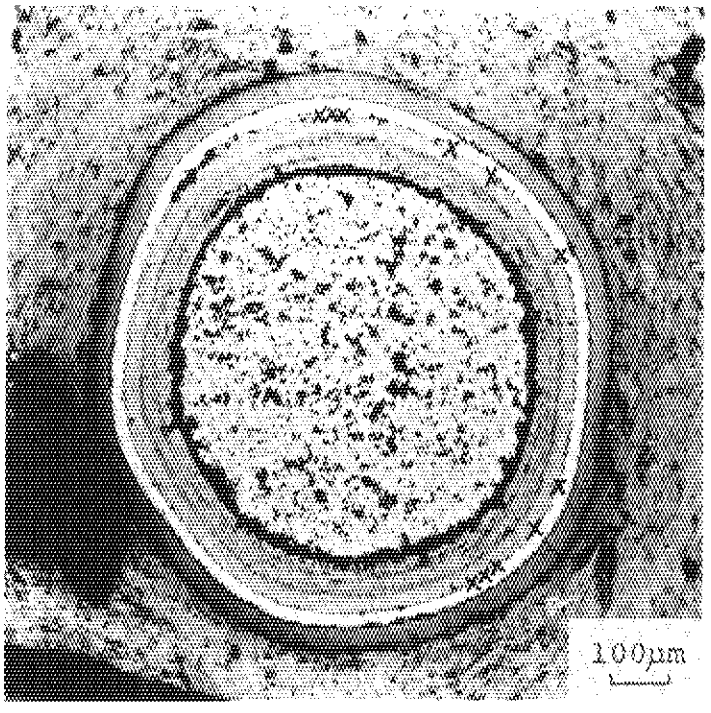

(b)

Fig. 3.33 Optical ceramographs of B-10 compact irradiated in 79LF-19A capsule. Symbol X indicates palladium accumulation positions. (a) Piece of B-10 compact; (b) B-10-1 particle.

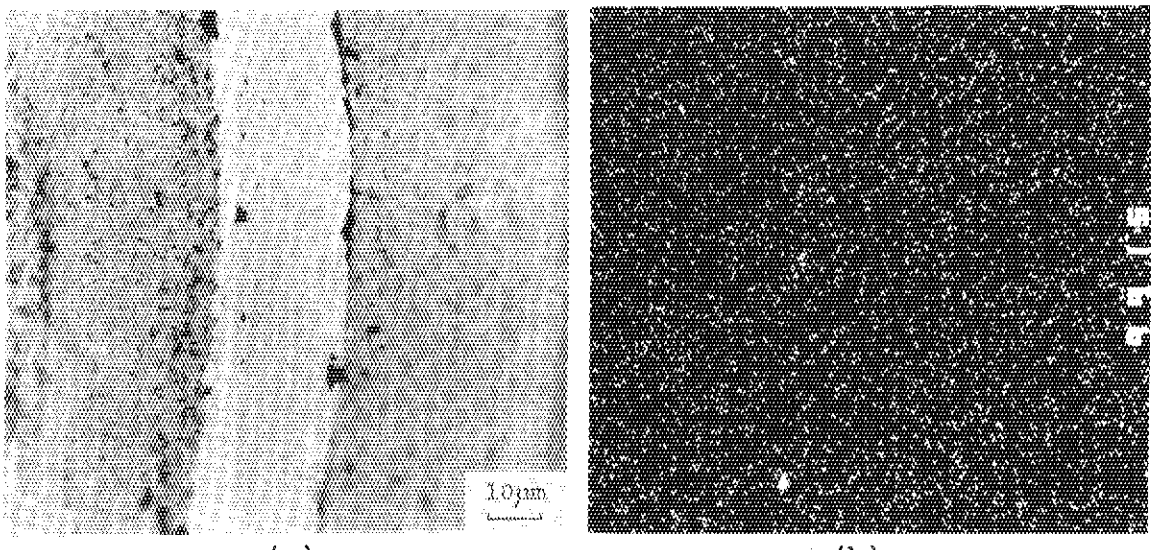

Fig. 3.34 Palladium accumulation at inner surface of the SiC layer of B-10-1 particle irradiated in 79LF-19A capcule. (a) Optical ceramograph; (b) Pd-Lα image.

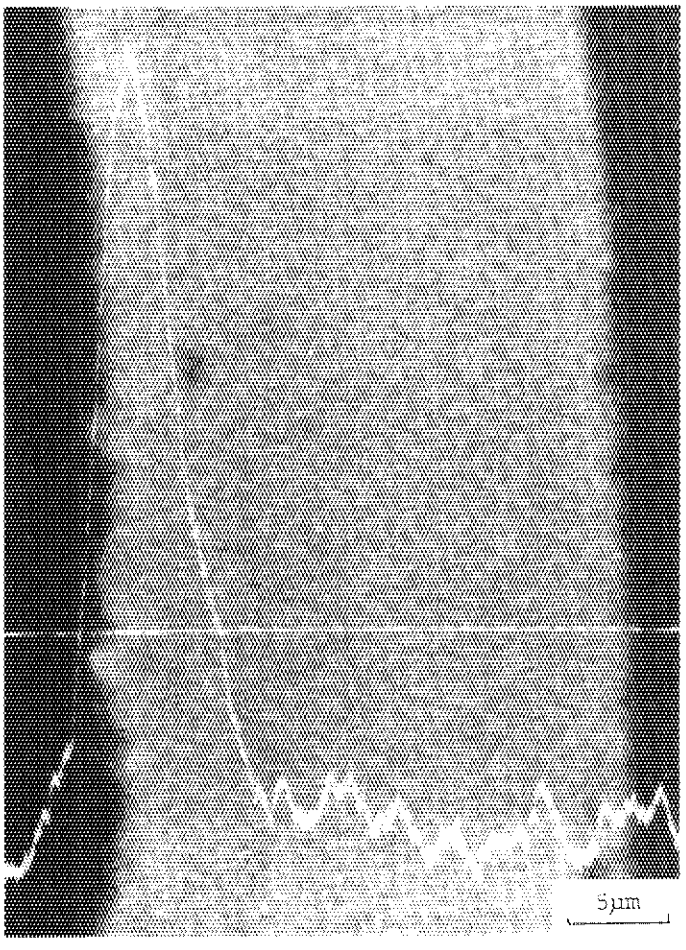

Fig. 3.35 Line scan for Pd-Lα X-ray across the coating layers of B-10-1 particle irradiated in 79LF-19A capsule.